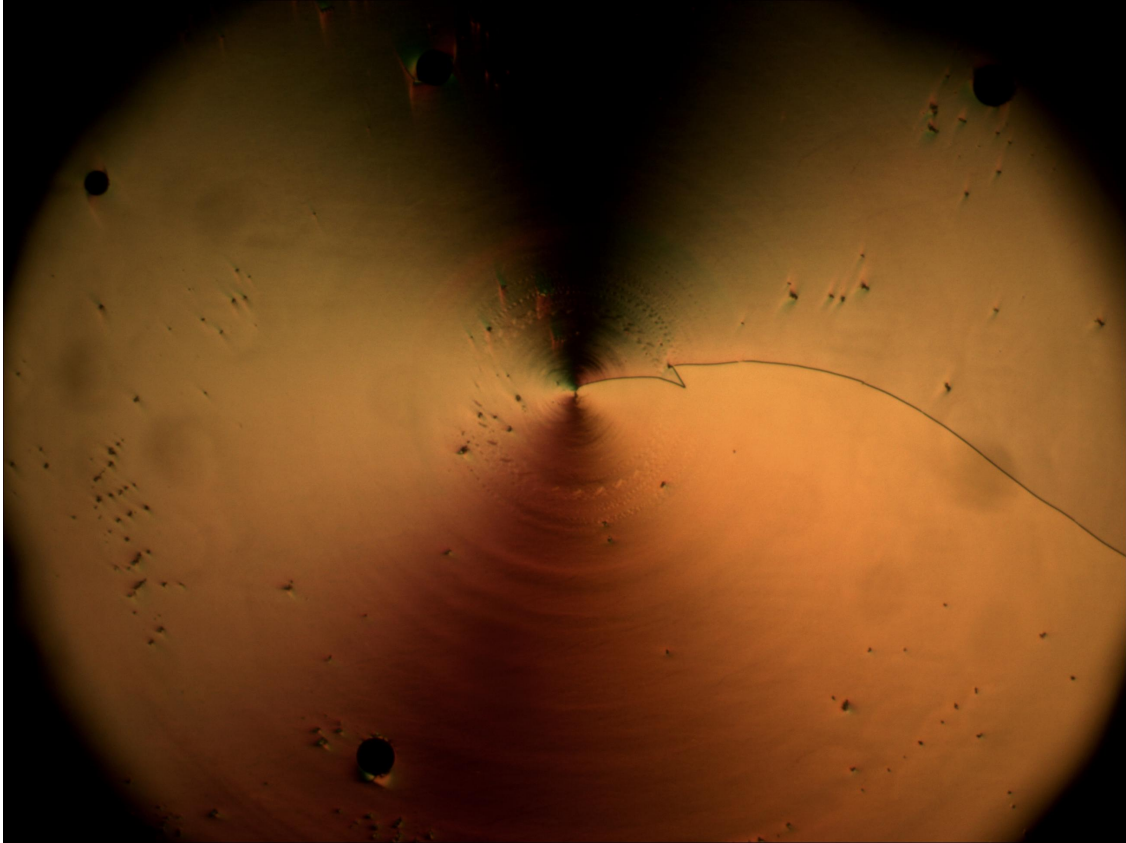
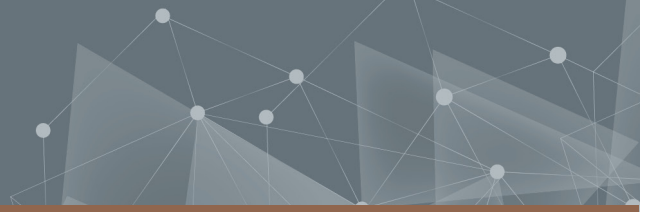




CHALMERS
UNIVERSITY OF TECHNOLOGY



Pitch Measurements on Chirally Doped Ferroelectric Nematics

Master's Thesis in Microtechnology and Nanoscience

PATRICK JONSSON

DEPARTMENT OF MICROTECHNOLOGY AND NANOSCIENCE

CHALMERS UNIVERSITY OF TECHNOLOGY
Gothenburg, Sweden 2023
www.chalmers.se

MASTER'S THESIS 2023

Pitch Measurements on Chirally Doped Ferroelectric Nematics

PATRICK JONSSON



CHALMERS
UNIVERSITY OF TECHNOLOGY

Department of Microtechnology and Nanoscience
Division of Electronics Materials and Systems
CHALMERS UNIVERSITY OF TECHNOLOGY
Gothenburg, Sweden 2023

Pitch Measurements on Chirally Doped Ferroelectric Nematics
PATRICK JONSSON

© PATRICK JONSSON, 2023.

Supervisor and Examiner: Assoc. Prof. Docent Per Rudquist, Department of Microtechnology and Nanoscience, Chalmers University of Technology

Master's Thesis 2023
Department of Microtechnology and Nanoscience
Division of Electronics Materials and Systems
Chalmers University of Technology
SE-412 96 Gothenburg
Telephone +46 31 772 1000

Cover: Image at the ferronematic phase of liquid crystal material RM734 doped with chiral dopant S811 in a circularly rubbed cell at 120 °C, the pitch is calculated from the azimuthal position of the disclination line when viewed through a polarised optical microscope with crossed polarisers.

Typeset in L^AT_EX
Printed by Chalmers Reproservice
Gothenburg, Sweden 2023

Pitch Measurements on Chirally Doped Ferroelectric Nematics
PATRICK JONSSON
Department of Microtechnology and Nanoscience
Chalmers University of Technology

Abstract

Following the recent discovery of the ferronematic liquid crystal phase, it is important to explore the material's properties as well as to devise methods of identification. In this report, an experimental method to measure the helical pitch of the ferronematic material RM734 doped with a chiral dopant S811 by use of the so-called circularly rubbed cell method is explored for the first time and compared to other methods. The method utilises a cell of two substrates linearly and circularly rubbed of which the pitch is measured from the resulting deviation angle of disclination lines induced by this particular geometry. The results showed that the pitch in the polar ferroelectric phase behaved similarly to that of the non-polar nematic phase but with a small change in magnitude at the phase transition to the polar phase. Phase transition temperatures could also be determined and a negative trend between the doping concentrations and transition temperatures for both the isotropic to nematic and nematic to ferronematic phases was observed. Finally, a first attempt was made at in-situ ultraviolet light-induced polymer stabilisation of the ferronematic liquid crystal by use of photoreactive monomers mixed into the liquid crystal. This attempt yielded inconclusive results as polymer stabilisation was not observed, yet there seemed to be some adverse effects on the liquid crystal.

Keywords: pitch, ferronematic, liquid crystal, circular alignment

Acknowledgements

I would like to thank my supervisor Per Rudquist for the excellent guidance and valuable inputs throughout the course of the project. I would also like to thank fellow student Ebba Grönfors for the helpful collaboration work between our projects. Finally, many thanks to family and friends for the continuous daily support.

Patrick Jonsson, Gothenburg, June 2023

List of Acronyms

Below is the list of acronyms that have been used throughout this thesis listed in alphabetical order:

CR	Circularly Rubbed
CRC	Circularly Rubbed Cell
<i>d</i>	Cell Gap
DI	Deionised
DMSO	Dimethyl Sulfoxide
<i>f</i>	Elastic Free Energy
Iso	Isotropic
ITO	Indium Tin Oxide
K_2	Elastic Twist Constant
LC	Liquid Crystal
LCD	Liquid Crystal Display
n	Director
N	Nematic
N_F	Ferronematic
N^*	Chiral Nematic
<i>p</i>	Pitch
POM	Polarised Optical Microscopy
PSLC	Polymer Stabilised Liquid Crystals
rpm	Rotations Per Minute
<i>S</i>	Strength of Disclination
s	Seconds
t	Time
T	Temperature
UR	Unilaterally Rubbed
UV	Ultra Violet

Contents

List of Acronyms	ix
List of Figures	xiii
List of Tables	xv
1 Introduction	1
1.1 Background	1
1.2 Problem Statement	1
1.3 Method	2
1.4 Key Results	2
2 Theory	3
2.1 Liquid Crystals	3
2.1.1 Liquid Crystal Phases	3
2.1.2 The Nematic and Ferronematic Phases	4
2.2 Defects, Disclinations and Deformations	5
2.3 Anisotropy and Birefringence	6
2.4 Polarised Optical Microscopy	6
2.5 Liquid Crystal Displays	7
2.5.1 Cholesteric Liquid Crystals and Pitch	8
2.5.2 Circularly Rubbed Cells	9
2.5.3 Pitch in Circularly Rubbed Cells	9
2.5.4 Pitch in the Ferronematic Phase	11
2.6 Polymer Stabilisation	12
3 Method	13
3.1 Cell Fabrication	13
3.1.1 Substrate Preparation	13
3.1.2 Polymer Preparation, Application and Brushing	14
3.1.3 Cell Assembly	14
3.1.4 Doping and Filling	16
3.2 Microscopy	17
3.3 Polymer Stabilisation	18
4 Results	19
4.1 Phase Transition Temperatures	19

Contents

4.2	Pitch Measurements	20
4.2.1	Calculations and Observations	22
4.3	Polymer Stabilisation	26
5	Conclusion	29
	Bibliography	31
A	Measurements of Deviation Angles	I

List of Figures

2.1	<i>Schematic depiction of the molecular alignments for the nematic, smectic A and smectic C phases.</i>	4
2.2	<i>Schematic representation of the molecular arrangements in the (a) nematic phase and (b) ferronematic phase, the molecular dipoles are indicated as red arrows.</i>	4
2.3	<i>Director configurations of three different types of disclination patterns. The grey areas show the dark bands that are observed when viewed under crossed polarisers. The crossed polariser directions are represented by the red arrows.</i>	5
2.4	<i>Schematic of the molecules in splay, bend and twist deformations.</i>	6
2.5	<i>Schematic of a polarising transmission light microscope.</i>	7
2.6	<i>Schematics showing molecular arrangement of N phase in a) parallel and b) antiparallel rubbing giving rise to a non-twisted structure. In the N_F phase the polarisation aligns with the rubbing direction causing c) non-twisted structure in parallel rubbing and d) left or right-handed twist in the structure for antiparallel rubbing.</i>	8
2.7	<i>Structure of a chiral nematic phase. The distance along the helical axis for the director to fully rotate 360° is known as the pitch.</i>	9
2.8	<i>Schematics showing twist deformations of nematic LC in a CRC when viewed from the top and pitch is a) infinite and b) finite. The top plate is UR and the bottom is CR.</i>	10
2.9	<i>Schematics showing twist orientations of CRC when viewed from the top and filled with a) pure ferronematic and b) doped ferronematic LC molecules. The top plate is UR and the bottom is CR.</i>	11
3.1	<i>Workflow for the manufacturing of CRCs used in the project, the magenta and yellow stages represent work inside and outside the clean-room respectively.</i>	13
3.2	<i>Schematics showing a) the glueing pattern of the cells on the substrate plates and b) the scribing patterns on the glueing pattern, the red and yellow lines representing two separate layers.</i>	15
3.3	<i>Schematic cross-section of the CRC cells. The grey circles represent spacers, bear in mind that these only exist in the glue and are not mixed in with the LC medium.</i>	15

3.4	<i>Image of a finished CRC cell, here the top and bottom cells are UR and CR respectively. The green arrow indicates the direction of the UR substrate.</i>	16
4.1	<i>Plots of the phase transition temperatures for different concentrations of S811 doped RM734 in the a) 1.5 μm and b) 4 μm thick CRC. The blue and red plots represent the transition from Iso to N and N to N_F respectively.</i>	19
4.2	<i>Images showing disclination lines of 0.9 wt% doped 1.5 μm CRC at different temperatures a) 170 $^\circ\text{C}$, b) 150 $^\circ\text{C}$, c) 130 $^\circ\text{C}$, d) 120 $^\circ\text{C}$, e) 115 $^\circ\text{C}$, f) 105 $^\circ\text{C}$, g) 95 $^\circ\text{C}$ and h) 85 $^\circ\text{C}$ for the cooling down of the cell. The white arrows indicate the disclination lines movement.</i>	21
4.3	<i>Figures showing a) 1.5 μm thick CRC filled with 0.9 wt% S811 in RM734 at 170 $^\circ\text{C}$ showing disclination line, image captured by the POM camera. b) Schematic representation of the POM image showing the director twist in the molecules.</i>	22
4.4	<i>Figures showing a) 1.5 μm thick CRC filled with 0.9 wt% S811 in RM734 at 120 $^\circ\text{C}$ showing disclination line, image captured by the POM camera. b) Schematic representation of the POM image showing the director twist in the molecules.</i>	23
4.5	<i>Plot of the predicted, observed and corrected disclination line angles in the 1.5 and 4 μm CRC.</i>	24
4.6	<i>Plots of the calculated pitch values from the observed and corrected disclination angles of the 1.5 and 4 μm CRC at different temperatures.</i>	25
4.7	<i>POM image of a 1.5 μm CRC filled with 3.0 wt% S811 in RM734 under crossed polarisers at 170 $^\circ\text{C}$.</i>	26
4.8	<i>POM images of 1.5 μm CRC filled with pure RM734, Irgacure 651 and RM82 at a) 150 $^\circ\text{C}$ and b) 110 $^\circ\text{C}$ before UV exposure.</i>	26
4.9	<i>POM images of 1.5 μm CRC filled with pure RM734, Irgacure 651 and RM82 at a) 150 $^\circ\text{C}$ and b) 110 $^\circ\text{C}$ after UV exposure.</i>	27
A.1	<i>POM images of the 1.5 μm CRC filled with 0.9wt% doping concentration at different temperatures a) 170 $^\circ\text{C}$, b) 150 $^\circ\text{C}$, c) 130 $^\circ\text{C}$, d) 120 $^\circ\text{C}$, e) 115 $^\circ\text{C}$, f) 105 $^\circ\text{C}$, g) 95 $^\circ\text{C}$ and h) 85 $^\circ\text{C}$. The dotted red line is the rubbing axis and the green line is an approximation for the disclination line. Using the circular protractor the angle is measured.</i>	II
A.2	<i>POM images of the 4 μm CRC filled with 0.9wt% doping concentration at different temperatures a) 170 $^\circ\text{C}$, b) 150 $^\circ\text{C}$, c) 130 $^\circ\text{C}$, d) 120 $^\circ\text{C}$, e) 115 $^\circ\text{C}$, f) 105 $^\circ\text{C}$, g) 95 $^\circ\text{C}$ and h) 85 $^\circ\text{C}$. The dotted red line is the rubbing axis and the green line is an approximation for the disclination line. Using the circular protractor the angle is measured.</i>	III

List of Tables

3.1	<i>Power, temperature and time settings for the preset program used in the megasonic bath.</i>	14
3.2	<i>Concentrations of chiral dopant S811 in RM734 for both the 1.5 and 4 μm thick CRCs that were tested.</i>	17
4.1	<i>Table showing the obtained deviation angles of the disclination lines and pitch for the 1.5 μm CRC at different temperatures of 0.9 wt% doping.</i>	23
4.2	<i>Table showing the predicted and observed deviation angles as well as resulting pitch for the 4 μm CRC at different temperatures of 0.9 wt% doping.</i>	24

1

Introduction

1.1 Background

The electro-optic effects of nematic liquid crystals have for many years provided the basis for the multi-billion dollar liquid crystal display industry. Recently, the discovery of previously speculated ferroelectric nematics - nematic liquid crystals with spontaneous polarity - has attracted great interest for their potential applications as well as fundamental physics. In order to understand and explore the potential applications of this phase it is important to derive methods of experimental identification for potential ferroelectric nematics.

The basic nematic liquid crystal phase is a three-dimensional orientationally ordered liquid. The average direction of the molecules is denoted by the director \mathbf{n} and for the nematic phase the director is invariant under sign reversal $\mathbf{n} = -\mathbf{n}$. The nematic phase's structure is well-studied and known to be non-polar [1]. However, in 2017 Nishikawa et al. [2] and Mandle et al. [3][4] discovered materials in which the nematic phase did not display the characteristic sign invariance. These materials, termed DIO and RM734 respectively, exhibited ferroelectric-like dipolar molecular associations. In 2020, subsequent research by Sebastián et al. [5] and Chen et al. [1] provided evidence that the phase in RM734 was indeed the ferronematic phase. Since then, many chiral ferronematic materials have been synthesised and studied [6]. Interestingly, there have been suggestions that the ferronematic phase should spontaneously form a helix even if the molecules are not chiral [7].

Following this, in 2021, Rudquist [8] demonstrated a direct method for experimental verification of a ferronematic liquid crystal phase by use of a single sample cell with two substrates linearly and circularly rubbed respectively. Determination of the ferronematic phase could then be derived from the orientation of the resulting disclination lines. In the report, Rudquist further suggested that in theory, the circularly rubbed cell method should be able to facilitate pitch measurements of the chiral ferronematic phase.

1.2 Problem Statement

The purpose of this project was to determine whether pitch measurements could be made on the ferronematic material RM734 doped with chiral dopant S811 by use of the circularly rubbed cell method. Although other methods exist, the circularly rubbed cell method is beneficial in that it works well at determining long pitches at low dopant concentrations. The project aimed to investigate the nature of pitch

measurements and if such helical structures can be polymer stabilised. Investigation of the nature of any potential pitch measurement strived to discover boundary conditions as well as parameters of influence. Questions sought to be answered were; what values of doping concentration will yield what pitch length? How can the pitch be regulated by other means such as temperature? What happens in the low concentration limit? These were parameters that were known for chiral nematics but had yet to be confirmed for the ferronematic phase [6].

To keep the scale of the project appropriate for the time and resources available, a few limitations were set. This included limiting the amount of pitch measuring techniques to only the circularly rubbed cell method as well as only trialling a select few doping concentrations of the RM734 and S811 dopant. Additionally, the project did not investigate the effects that different concentrations of polymer on the rubbed substrates would have on the pitch. Furthermore, it also left out any endurance trials of the RM734 material to repeated switching between the nematic and ferronematic phases. The most important limitation to bear in mind is that the project only measured pitch on the RM734 material and not any of the other known ferronematic materials. Thus it may be possible that the results of this material are not representative of all ferronematic materials. Future work should aim to investigate if the results from this study can be applied to other ferronematics.

1.3 Method

The circularly rubbed cell and polymerisation stabilisation methods used in the project were in large part derived from previous research. The main focus has been on applying these to the ferronematic material for the first time. The preparation of the cells in the circularly rubbed cell alignment was done in accordance with the technique developed by Suh et al [9] with the same manufacturing process as in Rudquist's [8] report. Polarised optical microscopy was largely used for the analytical work and a polymerisation attempt was made using a conventional ultraviolet light-exposure method [10].

1.4 Key Results

The results of the project suggest that pitch measurements can indeed be made on chirally doped ferronematic RM734 by use of the circularly rubbed cell method. They further indicate a negative trend between the doping concentrations and phase transition temperatures for both the isotropic to nematic and nematic to ferronematic phases. Furthermore, it was found that thinner cells would result in a shorter pitch. The results from the polymer stabilisation attempt were inconclusive as no definitive stabilisation was observed, yet the sample did experience a change in its disclination lines. Further inquiry into the stabilisation process is required.

The results obtained in this project have provided a deepened knowledge of the behaviour of ferronematic liquid crystals and identification methods, providing a basis for which further investigations into the properties of ferronematics can be made.

2

Theory

2.1 Liquid Crystals

Liquid crystals (LCs) are an intermediary state between the condensed phases of crystalline solids and amorphous liquids. Molecular complexes in a solid are ordered in both position and orientation, with the molecules constrained to occupy specific positions and pointing their molecular axes in specific directions. In a liquid, on the other hand, the molecules are disordered and free to diffuse randomly throughout the material with the molecular axes rotating in every direction. LCs have lower order and higher symmetry than a solid, yet a higher order and lower symmetry than a liquid. This means that the molecules in a LC diffuse about as much as molecules in a liquid, yet still maintain a degree of fluctuating orientational and sometimes even positional order, as for instance in smectic (layered) phases. Important to note is that the order of a LC is dynamic. This implies that the order of the LC is only observable on average. In most LCs, there is only a slight tendency for molecules to point more in one direction and to spend more time in one position than in another. The tendency of the molecules to point in a general direction is known as anisotropy (more on this in Section 2.3) and implies that the material's properties depend on the direction it is being measured in. These conditions allow LCs to share properties of both solids and liquids of which they famously find their use in the display industry [11][12].

2.1.1 Liquid Crystal Phases

Molecules of LC phases are usually rod-like, that is to say, one of the molecular axes is longer than the other two. This type of system is known as the calamitic LC phase. There are many calamitic LC phases but the three most prominent ones are the nematic (N), smectic A and smectic C phases depicted in Figure 2.1. For these phases, it is important that there is a certain level of rigidity over the core of the molecule's length in order to maintain an elongated shape for alignment interactions and ordered packing. Many calamitic LCs belong to the thermotropic LC group, where the phase is stable for certain temperatures. This category encompasses pure compounds and mixtures of compounds. In contrast to this is the lyotropic LC group. In this category, the molecules only form LC phases when mixed with a solvent. For these compounds, the concentration of the constituent solvent solution is more important than the temperature in determining the stable phase [11][12].

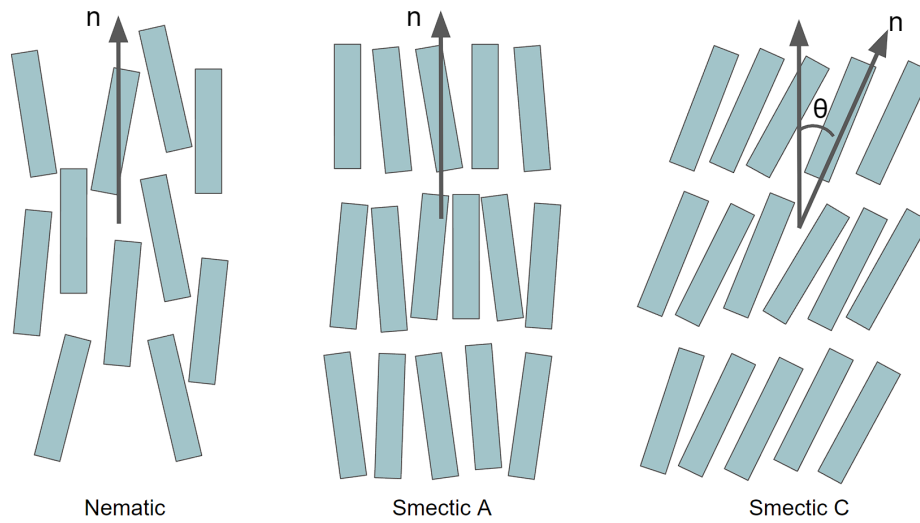


Figure 2.1: Schematic depiction of the molecular alignments for the nematic, smectic A and smectic C phases.

2.1.2 The Nematic and Ferronematic Phases

Of the most prominent calamitic LC phases, the N phase is the most structurally basic one. In this phase the molecular axes tend to point in one preferred direction as the molecules undergo diffusion, there is no positional order. As mentioned in Section 1.1, the average direction is known as the director \mathbf{n} and is invariant ($\mathbf{n} = -\mathbf{n}$) for the N phase since the preferred direction can be defined in either direction. Crucially, this is not the case for the ferronematic (N_F) material as it displays spontaneous polarity driven by the dipolar ordering of molecular dipoles in highly polar materials, see Figure 2.2 [1].

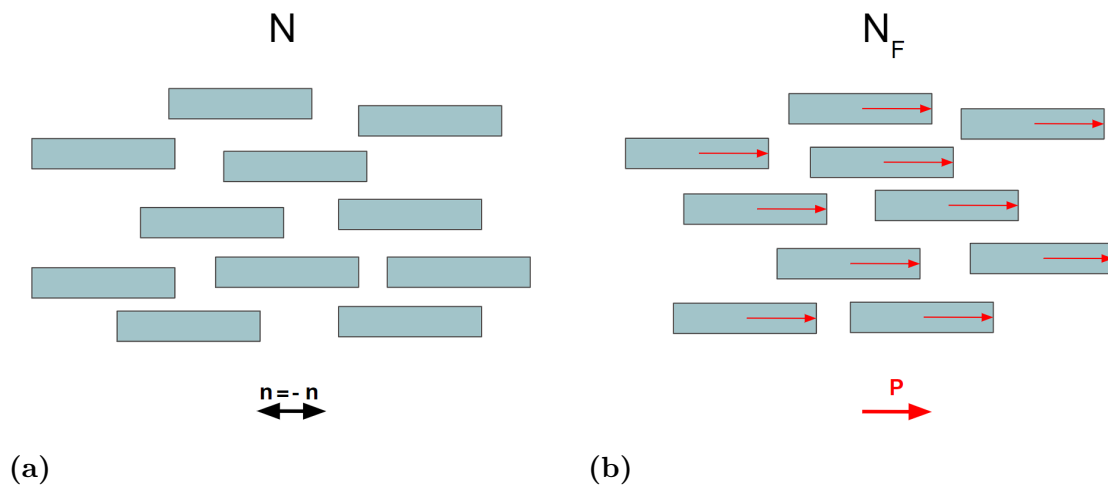


Figure 2.2: Schematic representation of the molecular arrangements in the (a) nematic phase and (b) ferronematic phase, the molecular dipoles are indicated as red arrows.

The N_F material in focus for this project is the calamitic compound 4-[(4-nitrophenoxy)carbonyl]phenyl-2,4-dimethoxybenzoate, better known as RM734, first synthesised by Mandle et al [3][4] in 2017 and supplied by the Boulder Group and University of Stuttgart. The exact mechanisms behind the N_F phase in RM734 are still ambiguous and uncertain. Mandle et al. and the Ljubljana group performed a series of physical studies in which they subsequently claimed that the phase is locally polar, but that on the macroscopic level, it is splay nematic; a modulated phase that is stabilized by local director splay [5][13][14][15]. However, in a following study Chen et al. [1] were unable to confirm the splay N phase. Instead, the study concluded that when cooling RM734 from the higher N phase temperature, the material would undergo a transition to a uni-axial N phase that is ferroelectric (the N_F phase).

The mechanisms behind the N_F phase in RM734 are not within the scope of this project, but it should be noted that the results presented here are more in alignment with the report by Chen et al. and that the splay nematic explanation would complicate the reasonings presented in this report.

2.2 Defects, Disclinations and Deformations

Typically, a liquid crystal contains many defects. These are points, lines or sheets in the sample in which the director is undefined, this means that the direction of the orientational order discontinuously changes when passing through one of these defects. Line defects, known as disclinations, are the most common defects to occur in liquid crystal samples and are of great significance to this project [16].

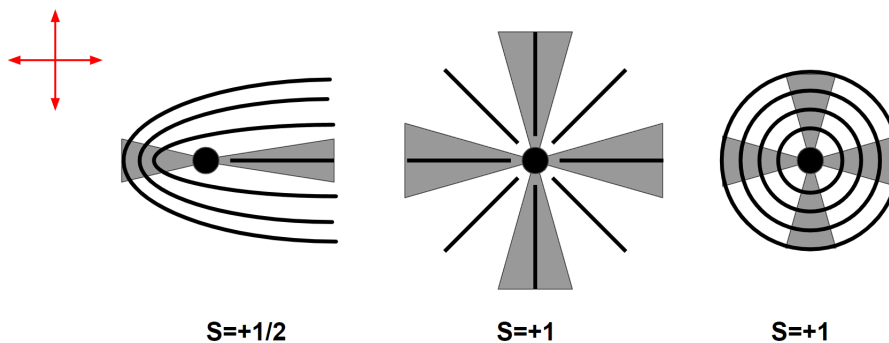


Figure 2.3: Director configurations of three different types of disclination patterns. The grey areas show the dark bands that are observed when viewed under crossed polarisers. The crossed polariser directions are represented by the red arrows.

The director configuration for some disclinations are shown in Figure 2.3. If S is the strength of the disclination, then when S is positive, the director undergoes a counterclockwise rotation when making a counterclockwise path around the disclination. If S is negative the director makes a clockwise turn when going counterclockwise around the disclination [11][16].

When a LC undergoes mechanical stress there are three deformations that can be considered; splay, twist and bend. These are curvature deformations of the director field and are coupled to an elastic free energy density. Schematic depictions of these deformations are shown in Figure 2.4.

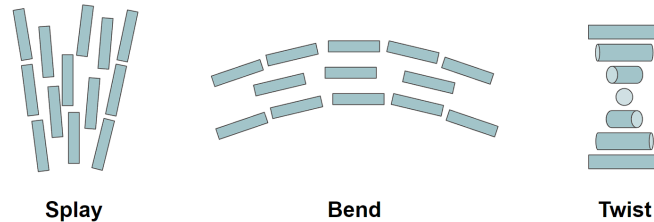


Figure 2.4: *Schematic of the molecules in splay, bend and twist deformations.*

2.3 Anisotropy and Birefringence

One of the most characteristic features of a LC material is that they are anisotropic, this means that the properties of the material depend on the direction as opposed to isotropic (Iso) materials, where the properties of a material are identical in all directions. For any material, light entering will experience a decrease in its wavelength and velocity by a factor known as the index of refraction. In an isotropic material, the index of refraction has a single value. However, since LCs are anisotropic, measurements on the refractive index will instead give different results depending on the direction in which it is being measured along. Thus anisotropy in LCs affects the propagation of light through the material resulting in varying indices of refraction known as birefringence. The ability of LCs to exhibit birefringence is crucial for the material's optical behaviour and is of great importance in industrial applications [11][17].

2.4 Polarised Optical Microscopy

There are a multitude of different techniques and equipment used to perform research on liquid crystals. Some of these techniques probe the liquid crystal material itself whereas other techniques investigate the physical properties of the material. Polarised optical microscopy (POM) is a probing technique of particular interest for this project as it enables the observation of the LCs birefringence and is perhaps one of the most universal techniques used in liquid crystal laboratories.

The POM is very similar to traditional microscopes in function and composition but possesses an analyser above the objective and a polariser beneath the rotatable stage, see Figure 2.5. The POM is also often accompanied by a heating/cooling unit connected to a hot stage that is placed on the rotatable stage. The LC sample placed between the crossed polarisers is in a temperature-controlled environment, and as such the POM makes it easy to measure the temperature at which phase transitions occur.

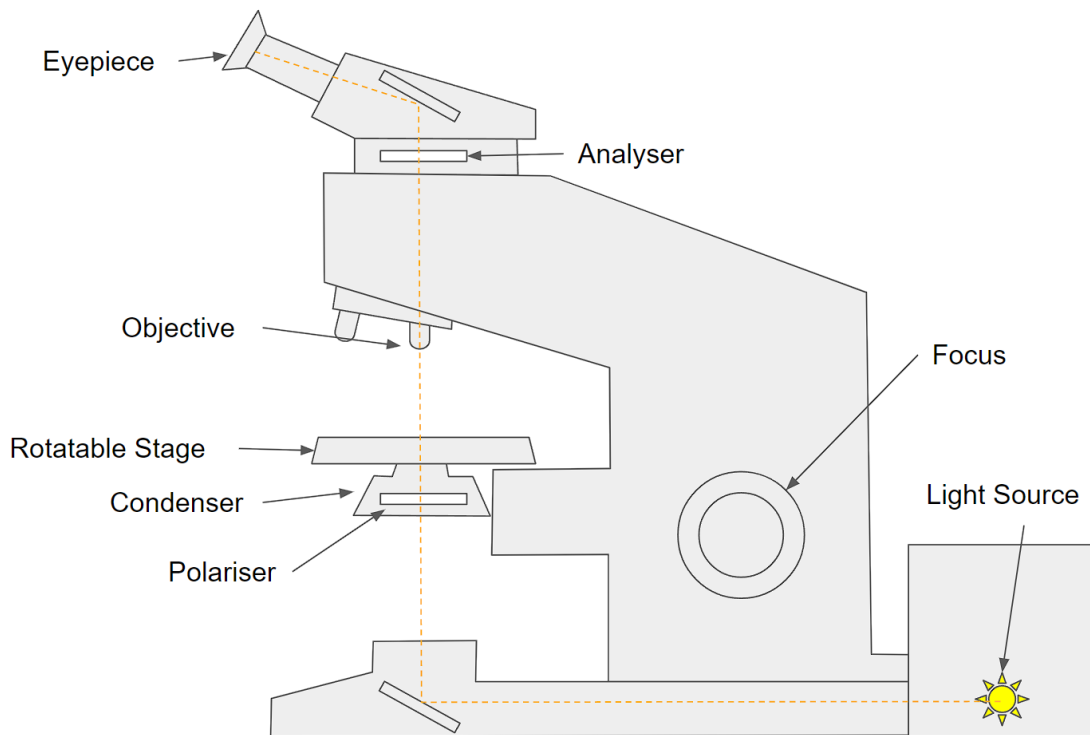


Figure 2.5: *Schematic of a polarising transmission light microscope.*

The POM is useful as when viewed between crossed polarisers, the LC will appear dark anywhere the director or projection of the director is orientated in parallel to the transmission axis of one of the polarisers, in all other orientations the LC will be bright and achieve its brightest state when the director is perpendicular to the optic axis along the viewing director [11].

2.5 Liquid Crystal Displays

Liquid crystal displays (LCDs) are the most prominent use of LCs. In a typical LCD cell, the equilibrium state is determined by the boundary conditions of the two substrate cells and the elasticity of the LC. In the N phase, the rubbing at the two surfaces, whether parallel or antiparallel, will produce non-twisted director fields as depicted in Figure 2.6a) and b). If the cell is twisted, that is to say, the rubbing directions are not colinear and at angles other than 0° or 180° , there will be a director twist between the surfaces [18]. The N_F phase exhibits fundamentally different director fields when the rubbing directions are antiparallel. In the N_F phase, the molecules will align with the spontaneous polarisation parallel to the rubbing direction [19]. The consequence of this is that in the antiparallel configuration, the director will experience a 180° twist between the surfaces, Figure 2.6d), with an equal affinity for left or right handed twist. For the parallel orientation there will be a non-twisted state similar to the N phase, Figure 2.6c). In the twisted alignment, the N_F phase should adopt the handedness with the smallest twist matching the rubbing [20].

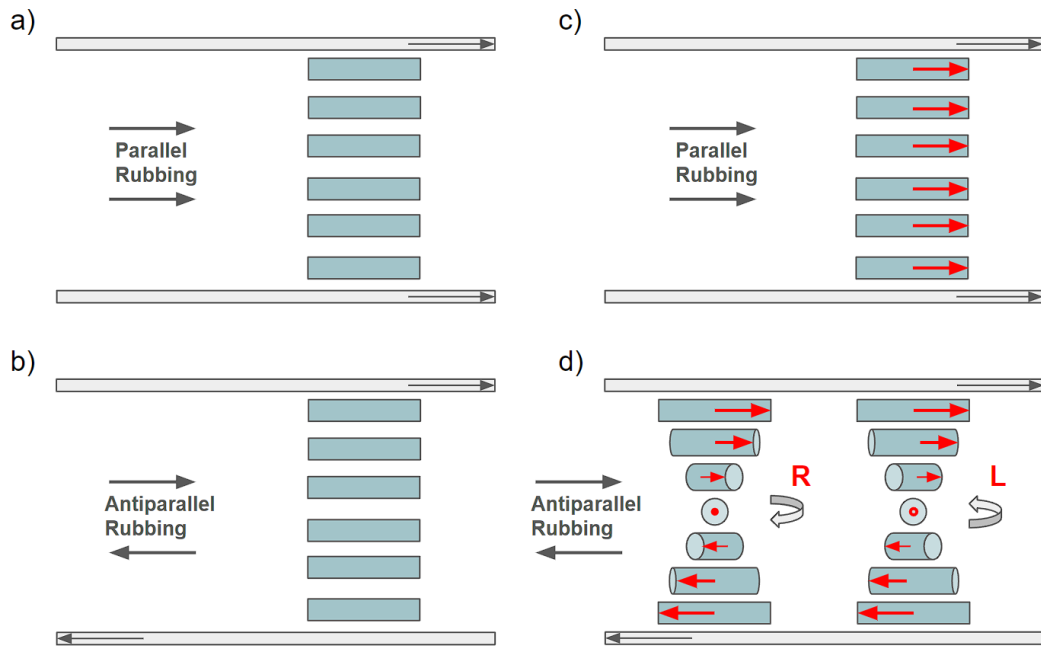


Figure 2.6: Schematics showing molecular arrangement of N phase in **a)** parallel and **b)** antiparallel rubbing giving rise to a non-twisted structure. In the N_F phase the polarisation aligns with the rubbing direction causing **c)** non-twisted structure in parallel rubbing and **d)** left or right-handed twist in the structure for antiparallel rubbing.

2.5.1 Cholesteric Liquid Crystals and Pitch

If the LC molecules that make up the material are chiral (lack of inversion or reflection symmetry) they will possess a director that rotates in a helical fashion about an axis perpendicular to the director as depicted in Figure 2.7. This type of phase is known as the cholesteric liquid crystal phase since many of the first compounds that possessed this phase were derived from cholesterol. Due to their chirality, they are sometimes also referred to as the chiral nematic phase (N^*).

The variation of the director tends to be periodic and the distance along the helical axis for the director to rotate by 360° is known as the pitch (p). The pitch of a N^* phase can be as short as 100 nm and the structure repeats itself every half pitch due to the director invariance. Mixing left and right-handed versions of the same chiral dopant in different concentrations will change the dominant handedness of the pitch. A racemic mixture possesses an infinite pitch [11].

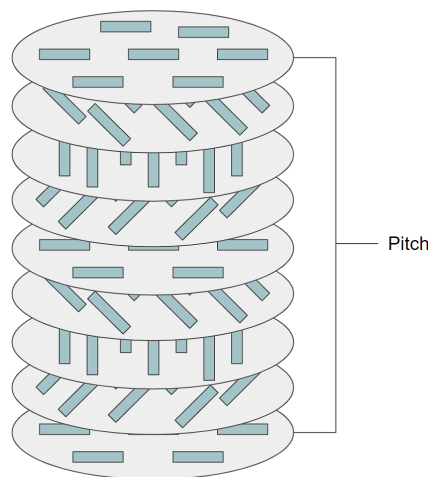


Figure 2.7: *Structure of a chiral nematic phase. The distance along the helical axis for the director to fully rotate 360° is known as the pitch.*

2.5.2 Circularly Rubbed Cells

Circularly rubbed cells (CRCs) are a technique used to measure the cholesteric pitch of LCs with a homogeneous circular geometry developed by Suh et al [9]. The technique determines the pitch from the angular deviation of the disclination line created by the geometry. The CRC consists of two rubbed glass plates placed parallel to each other, one of which is unidirectionally rubbed (UR) and the other which is circularly rubbed (CR). The principal concept in use with this technique is that LC molecules on a treated surface will tend to align along the rubbing direction. This means that on the UR surface, the molecules will align along the rubbing direction whilst on the CR surface they will form concentrically around the centre of rubbing. Therefore, as the molecules align along the rubbing directions, there will occur twist deformations in the cells. Some of which will produce disclination lines that will be characteristic of their phase [8][9].

2.5.3 Pitch in Circularly Rubbed Cells

Consider a CRC filled with a N LC with no chirality as schematically shown in Figure 2.8a). Note here that the top plate is UR and the bottom plate is CR, henceforth this will be the convention for all cells. Alongside the y -axis, there is no twist in the molecular director as the molecules on both the UR and CR surfaces are aligned with the x -axis. However, at all other positions of an angle θ to the x -axis, there will be a uniform twist in the director by an angle of $\pi/2 - \theta$ when going from the UR to the CR surface. In the case considered the direction of the twist, clockwise or counterclockwise (right and left-handed respectively), are equally probable and the $y=0$ (rubbing axis) separates the two twist domains which will appear as a disclination line [9].

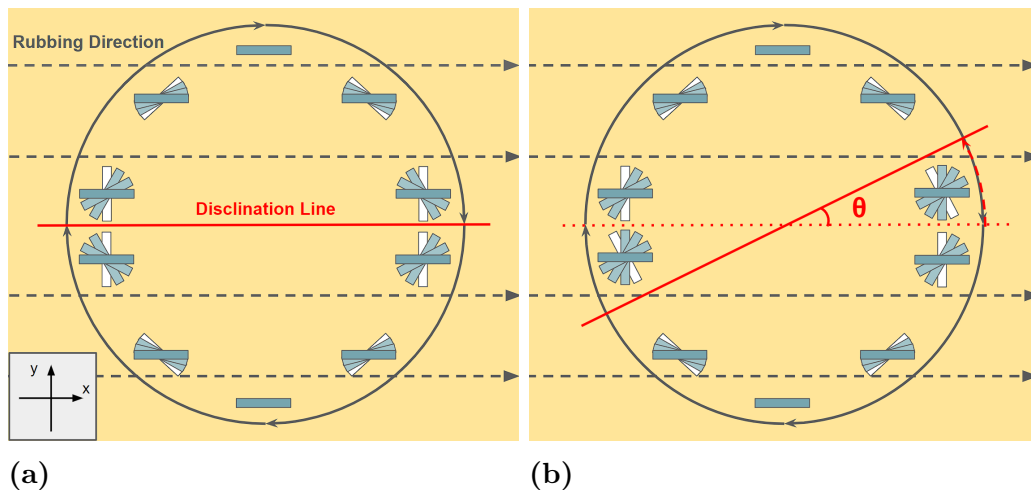


Figure 2.8: Schematics showing twist deformations of nematic LC in a CRC when viewed from the top and pitch is **a)** infinite and **b)** finite. The top plate is UR and the bottom is CR.

Now consider the CRC filled with a doped cholesteric LC of a pitch p , with helicity in the counterclockwise direction ($p < 0$). As shown in Figure 2.8b), the counterclockwise twist has lower elastic energy and as a consequence, the two domains of opposite twist will no longer meet at the rubbing axis. Instead, a plane at an angle θ from the rubbing axis acts as the symmetry plane where the disclination line will appear. The molecules are rotated $(\pi/2 - \theta)$ clockwise in one region and $(\pi/2 + \theta)$ counterclockwise in the other. Thus, the variation of the pitch will be reflected in the angle of the deviation that the disclination line has from the rubbing axis. It is worth noting that if the pitch is negative, this will be reflected in a negative deviation angle about the x-axis.

The relationship of the disclination deviation angle and the pitch is obtained from the elastic free energy (f) as follows [9]:

$$f = \int_0^d K_2 \left(\frac{\delta\phi}{\delta z} - q \right)^2 dz \quad (2.1)$$

where K_2 is the elastic twist constant, ϕ the azimuthal angle of director twist from the rubbing axis, z the axis normal to the surface of the cell and $q = 2\pi/p$. At fixed temperatures the pitch is constant, thus when under no external fields $\delta\phi/\delta z$ is uniform and f can be rewritten as:

$$f = K_2 \left(\frac{\phi_T}{d} - q \right)^2 d \quad (2.2)$$

where ϕ_T is the total azimuthal angle of twist from one surface to the other and d is the cell gap. If it is assumed that the disclination line makes an angle θ to the rubbing axis, then the molecules on either side should have the same free energy when in equilibrium. If the system is unbalanced, the disclination line should move to reach a stable equilibrium condition. Since $\phi_T = \theta + \pi/2$ and $\phi_T = \theta - \pi/2$ when clockwise and counterclockwise respectively, then:

$$\left(\frac{\theta + \pi/2}{d} - q\right)^2 = \left(\frac{\theta - \pi/2}{d} - q\right)^2 \quad (2.3)$$

which in turn yields the relationship between the disclination line's deviation angle θ and p :

$$\theta = \frac{2\pi d}{p} \quad (2.4)$$

Worth noting is that the angles θ and $\theta + n\pi$, where n is an integer, although corresponding to two different pitches will display the same apparent position of the disclination line. As such, integral multiples of π rotations are indistinguishable from each other and cannot be uniquely determined. Therefore the amount of rotations that the disclination line has experienced in the cell is of importance. This is fairly straightforward for the case when $\theta < 2\pi$ and the pitch is large. But is more difficult when $\theta \gg 2\pi$ and the pitch is very small. In the case of this, a thinner cell must be used.

2.5.4 Pitch in the Ferronematic Phase

Consider now the same cell, but filled with LC of the N_F phase instead. Since the polar N_F phase orients with the polarisation along the rubbing directions, there will be a non-twisted director where the UR and CR rubbing directions are in parallel. When moving clockwise or counterclockwise from this location, there is a twist that increases continuously down to the opposite end where the rubbing directions are antiparallel. At this position there is a discontinuous change in twist between the right and left-handedness, giving rise to one disclination line as opposed to the two in the N phase. This N_F disclination line is therefore normal to the linear rubbing direction as opposed to along the rubbing direction in the N phase.

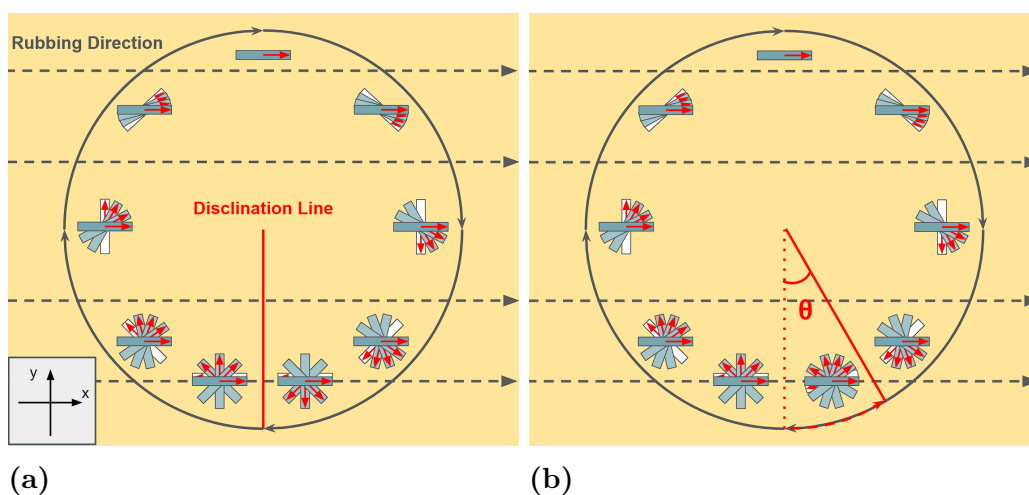


Figure 2.9: Schematics showing twist orientations of CRC when viewed from the top and filled with **a)** pure ferronematic and **b)** doped ferronematic LC molecules. The top plate is UR and the bottom is CR.

Following this, in theory, when the N_F material is doped with a chiral dopant the N_F phase CRC should behave similarly to that of the N phase CRC in that the disclination line will appear at a deviation angle θ as in Figure 2.9b). The pitch would then be calculated from Equation 2.4.

2.6 Polymer Stabilisation

Polymer stabilisation is a method used to stabilise the structure and properties of a LC [10]. Polymer stabilised liquid crystals (PSLCs) are generally formed by dissolving a small amount of an anisotropic and photoreactive molecule into a LC matrix. The spontaneous LC order is then transferred to the mixture and once oriented into the desired state the molecules are polymerised through irradiation with ultraviolet (UV) light. The resulting polymer network is then a stable structure of the LC phase it was formed in. This project uses Ciba Irgacure 651 photoinitiator as the photoreactive molecule and RM82 as the LC matrix. Note that here the "RM" in RM82 stands for "Reactive Monomer" and not "Richard Mandle" as in RM734.

3

Method

This chapter describes the fundamental methods and experimental techniques used in the project. Whilst most of these techniques were already established methods utilised in previous studies, they had not yet been fully realised for the N_F phase [8][9][10]. The project was essentially divided into three stages; cell fabrication, microscopy and polymer stabilisation. The CRCs were first manufactured before observation could be done under the microscope. Following this, an attempt at polymer stabilising the cells was made.

3.1 Cell Fabrication

This project had extensive use of the CRC method as described in section 2.5.3 and these were purpose-built for the sake of this project. The general workflow for the manufacturing and analysis of these cells is outlined in Figure 3.1:

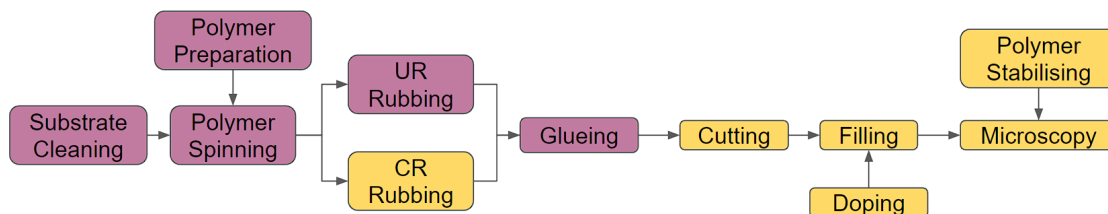


Figure 3.1: Workflow for the manufacturing of CRCs used in the project, the magenta and yellow stages represent work inside and outside the cleanroom respectively.

3.1.1 Substrate Preparation

To begin with, the CRCs were prepared from 1.1 mm thick 3x3 inch soda-lime glass substrates coated on one side with an 80 nm thick layer of Indium Tin Oxide (ITO). The preparation of the substrates took place in the MC2 cleanroom at Chalmers University of Technology with the hopes of providing a dust-free environment that minimised eventual contamination of the substrates, thus improving the accuracy of the results. Before the substrates were prepared, identification of the ITO sides was required as it would not be possible later on in the preparation stage. This was easily done by checking for the presence of a current with an Ohmmeter as the ITO side would be conductive. Once confirmed the substrates were loaded onto a carrier with the ITO sides facing one direction for easy identification. This carrier of substrates was cleaned in a megasonic bath. The bath was first filled with 2 L

of deionised (DI) water before 1.2 L of 25 wt% ammonia was added. After this, a further 2 L of DI water was added followed by 1.2 L of 30 wt% hydrogen peroxide (H_2O_2) and then a final dose of 2 L DI water. The substrates were placed onto an 8 cm high "table" at the bottom of the bath and ran on a preset program for 10 minutes, four times. The settings for this program are listed in Table 3.1.

Power	100
T_{set}	70
T_{min}	50
T_{max}	75
t	600 s

Table 3.1: *Power, temperature and time settings for the preset program used in the megasonic bath.*

Between each run, the carrier was washed with DI water in quick dump and rotated 90° so as to clean the entire substrate properly. The cleaned substrates were then dried in a centrifugal rinser dryer and baked in an oven at 110 °C for approximately one hour.

3.1.2 Polymer Preparation, Application and Brushing

The polymer was prepared from a preparation of 0.5% solution of PI2610 polyimide in Dimethyl Sulfoxide (DMSO), which had been mixed together for 3 hours. The polymer solution was spin-coated for 30 seconds at 5000 rpm with an acceleration of 2500 rpm/s onto the ITO side of the cleaned glass substrates. After which they were heated for 1 min at 100 °C on a heating plate to remove any remaining solvent. The substrates were then placed on a grooved Al plate which underwent hardening in an oven at 300 °C for approximately 3 hours. The oven was first heated to 250 °C as it was prone to overshooting the target temperature during heating. After hardening, the substrates were cooled to room temperature before the brushing process on the buffing machine. Brushing was done with a velvet cloth of 12 cm in diameter at 1000 rpm with a speed of 30 mm/s, for 2 brushing passes. The buffing machine only yielded substrate plates with the UR alignment as it lacked the configuration required to produce CR plates. These substrates were instead rubbed by a velvet cloth attached to a flat spinning chuck, which was delicately pressed against the substrate. This setup is essentially a drill with velvet cloth replacing the drill point. Due to the rudimentary nature of this equipment, the rpm and pressure applied were difficult to control and so varied from plate to plate but nevertheless yielded an effective CR alignment. Throughout both the UR and CR process, the direction of rubbing is noted on the plates by use of markers.

3.1.3 Cell Assembly

With the CR and UR plates rubbed accordingly, they were glued together to complete the CRC cell. This took place back in the cleanroom on a modified Stepcraft 210 desktop system self-assembly kit. A mixture of Norland optical adhesive 68 glue

and 1.5 respective 4 μm glass spacers was dispensed onto the rubbed ITO side of the UR plates with the pattern depicted in Figure 3.2a). This pattern yielded 25 manageable 12.5x12.5 mm cells with cell thicknesses of 1.5 and 4 μm respectively.

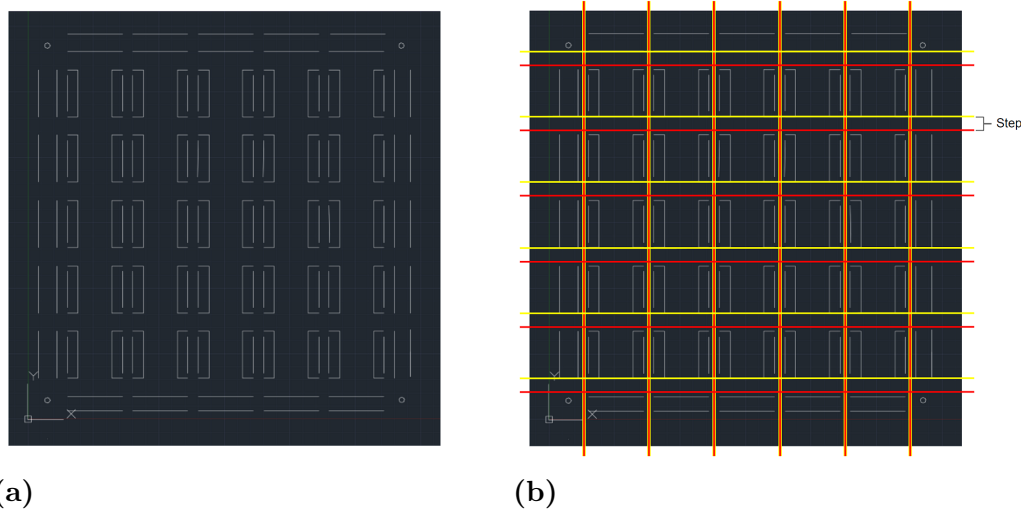


Figure 3.2: Schematics showing **a)** the glueing pattern of the cells on the substrate plates and **b)** the scribing patterns on the glueing pattern, the red and yellow lines representing two separate layers.

The UR and the CR plates were then aligned and pressed together with the ITO sides facing each other on a Cipsosa aligner and assembler, 4 seconds of UV exposure provided temporary hardening. The assembled substrate was then vacuum sealed in a plastic bag by a vacuum packer and placed in a UV illumination box for 10 minutes for a more permanent hardening. After hardening the assembled substrate plates were cut into the 25 cells as set by the glueing pattern. This involved a simple process of scribing lines onto the cell surface with a diamond-edged point. The lines were then cracked open. An important step in this process was to scribe the opening sides of the cell in such a way that there is a "step" in the cell as shown in Figure 3.3.

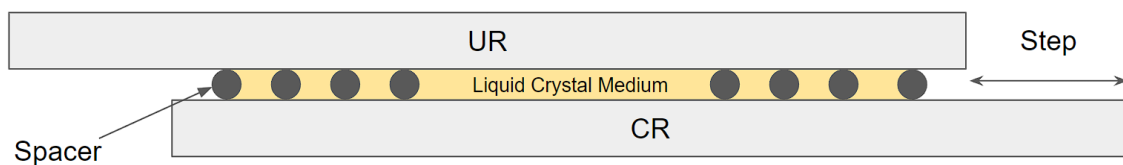


Figure 3.3: Schematic cross-section of the CRC cells. The grey circles represent spacers, bear in mind that these only exist in the glue and are not mixed in with the LC medium.

This was done by scribing the top and bottom substrate plates slightly offset to each other on the opening sides of the cell. See the horizontal yellow and red lines in Figure 3.2b).

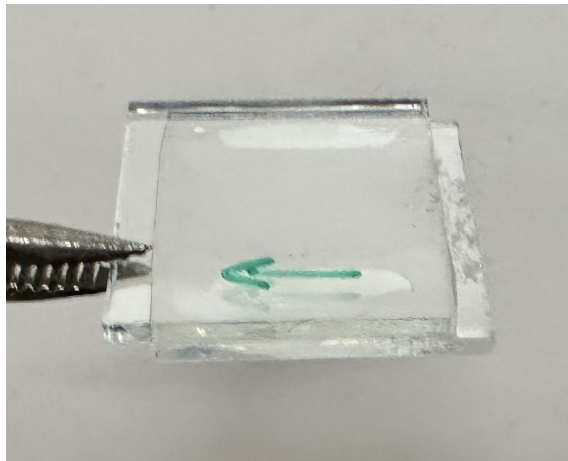


Figure 3.4: Image of a finished CRC cell, here the top and bottom cells are UR and CR respectively. The green arrow indicates the direction of the UR substrate.

Figure 3.4 shows an image of a finished CRC with the top and bottom substrates UR and CR respectively as per this project’s convention. Also seen in this figure is the step in the cell which was used for loading the doped RM734 powder as will be discussed in the following section.

3.1.4 Doping and Filling

The RM734 material was doped with the chiral dopant S811 purchased from Merck in order to induce chirality to the material. The project aimed to trial multiple concentrations to investigate the effect the doping concentration had on the pitch. As such, an initial batch was made with 8.9 wt% doping concentration. This was then diluted to make the smaller concentrations that were tested.

At the start of the project, access to the RM734 material was limited (perhaps only 200 mg available) and as such mixing low concentrations of RM734 and S811 with high accuracy proved difficult since extracting singular grains of powder was almost impossible. Therefore, the concentrations tested were randomly acquired. Weighing the materials took place in their powder state and was done on a thin glass plate with a folded piece of tape as a handle for transporting the sample. A small amount of 8.9 wt% doped batch material was placed on the glass plate and weighed on a scale. Pure RM734 was then added in rough amounts to dilute the concentration to a lower figure. The two powders were then mixed together in their liquid isotropic phase on a heat plate before being allowed to cool back down to the powder state. Table 3.2 shows the doping concentrations that were tested in this project for both the 1.5 and 4 μm thick CRCs.

The relative error in the weighing process was calculated from:

$$\frac{\Delta e}{e} = \frac{\Delta m}{m} + \frac{\Delta w}{w} \quad (3.1)$$

where e is the relative error, m the weight and w the losses from handling of the material. For the 8.9 wt% batch concentration, a total of $m=0.009$ g of RM734 and

S811 material was used. The scale had an absolute error of $\Delta m = 0.0001 \text{ g} = \Delta w$ and if eventual losses in the handling of the material were estimated to $w = 0.001 \text{ g}$, then the relative error was roughly 11% in the weighing process.

Cell thickness (μm)	Doping Concentrations (wt%)						
4	0	0.9	2.4	3.0	3.3	4.9	6.3
1.5	0	0.9	2.0	2.2	3.0	-	-

Table 3.2: Concentrations of chiral dopant S811 in RM734 for both the 1.5 and 4 μm thick CRCs that were tested.

Filling of the CRCs were similarly done at the isotropic phase. The CRCs were placed on a heater and heated to the temperature at which RM734 was isotropic, at around 190°C [20]. The doped RM734 materials, in powder form, were then placed on the step of the CRCs, as depicted in Figure 3.3, upon which they would melt. Through capillary force interaction, the cells were filled with the doped material. This final step concluded the preparation of the CRCs with doped RM734 material and they were then ready to be observed under the POM.

3.2 Microscopy

Observation of the cells was done with a POM (see Section 2.4) and a hot stage. The filled CRC was placed inside the hot stage and positioned under the POM objective, between the analyser and polariser. The CRC was then heated to 190°C as the starting temperature. It was then cooled down at a predetermined cooling rate. In this case, $20^\circ\text{C}/\text{min}$ was primarily used for determining the rough value of the phase transition temperatures and $0.6^\circ\text{C}/\text{min}$ was used for more precise measurements. The phase transition temperatures for the cooling process were measured for all concentrations of both CRC thicknesses as listed in Table 3.2. For this study, the transition from the Iso to N phase was calibrated to when the first sets of nematic "droplets" appeared. The N to N_F phase was determined to occur when the LC area first began to display disturbance and the disclination lines began to move towards the N_F configuration [21]. This was at times difficult to determine exactly as it depended entirely on judgment by the eye and the disclination line's movement could be very slow. It is due to this that the slower $0.6^\circ\text{C}/\text{min}$ rate was used so that the transition would not be missed.

7 doping concentrations were measured for the 4 μm thick CRC and 5 for the 1.5 μm , see Table 3.2. Only the 0 and 0.9 wt% doping concentration were measured for both the 1.5 and 4 μm thick cells in order to calibrate the method and to determine handedness. To measure the pitch, the samples were cooled to a set temperature and images of the resulting disclination lines were taken with the system's camera. The rubbing axis was used as the starting point for measuring the angle of deviation θ that the disclination lines made. The pitch could then be calculated according to Equation 2.4. To begin with, the disclination angles were measured for the 1.5 μm thick CRC and the pitch was calculated. These pitch values were then used to predict the expected deviation angle for the 4 μm thick CRC which was then

confirmed experimentally. Here, the problem of calibration arose as it appeared that the disclination lines had performed an integer multiple of π rotations, see Section 2.5.3. Therefore corrections had to be made by adding half rotations to the angles obtained.

3.3 Polymer Stabilisation

As a final point, an attempt to polymer stabilise the LC in the CRC by using a photoreactive dispersion and UV radiation as described in Section 2.6 was made. For this, 10.1 wt% of Ciba Irgacure 651 photoinitiator in RM82 was prepared as the photoreactive solution. This solution was then further mixed with pure RM734 to a concentration of 4.2 wt% photoreactive solution in RM734. Following this, and similarly to the main body of work in this project, the 4.2 wt% solution was loaded onto a CRC on a heater and filled by capillary force. It was then placed on the hot stage and heated to a specified temperature. Once this temperature was reached and the disclination line reached its equilibrium position, the heater was moved to, and exposed to UV light from a Leica UV lamp (for fluorescence microscopy). The exposure lasted for 15 minutes upon which it was then returned to the POM for analysis.

4

Results

This chapter presents and examines the results obtained from the study in three parts; the identification of phase transition temperatures, the measuring of the pitch from the deviation angle of disclination lines and finally the results of the polymer stabilisation attempt.

4.1 Phase Transition Temperatures

Using the method mentioned in Section 3.2 and the parameters set by it, the phase transition temperatures for the Iso-N and N-N_F transitions were identified. Figure 4.1 shows the plotted trends of transition temperatures for different doping concentrations acquired for the 1.5 and 4 μm thick cells.

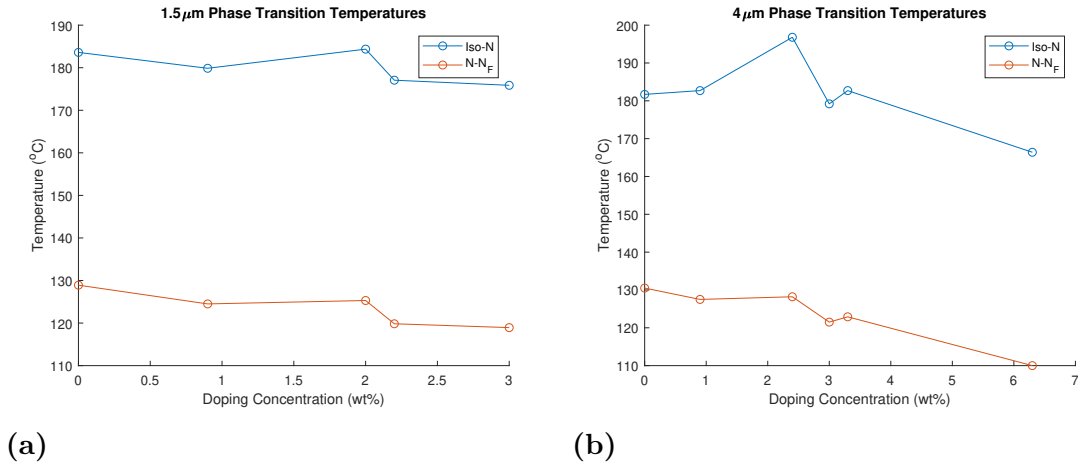


Figure 4.1: Plots of the phase transition temperatures for different concentrations of S811 doped RM734 in the **a)** 1.5 μm and **b)** 4 μm thick CRC. The blue and red plots represent the transition from Iso to N and N to N_F respectively.

As can be seen, there is a negative trend for the phase transition temperatures as doping concentration increases. In general, all of the doped RM734 samples were observed to have lower phase transition temperatures than in RM734's pure form (Iso-N=189 $^{\circ}\text{C}$ and N-N_F=133 $^{\circ}\text{C}$). This is in line with other studies and is to be expected when mixing a material of lower phase transition temperature with one that has a higher [6][22]. Specifically, Feng et al. [6] have reported similar phase transition temperatures as observed here, although the values obtained in this project are

slightly lower on average compared to Feng's study.

Furthermore, in both the 1.5 and 4 μm CRCs, the 0.9 wt% concentration does not follow the negative trend and has a lower phase transition temperature than the higher doping concentrations. Whilst the explanation for this discrepancy could be that the low concentration has some physical effect on the material, it should be noted that this concentration was made from a different batch of RM734 material and as such there could be slight differences in the manufacturing quality.

Another outlier in the negative trend lies with the 2.4 wt% doping concentration for the 4 μm CRC. This point is much higher than expected, but this is likely to be because of an error in the dopant weighing. It is possible that the concentration was inadvertently mixed incorrectly or had been contaminated. Therefore, repeated measurements should be made to achieve higher accuracy. Also worth noting is that for both the plots of CRC thickness, the transition temperatures of the 8.9 wt% batch concentration have been omitted as in this concentration the N-N_F transition could not be determined. This is because the material began to crystallise before it could reach the N_F phase or that the phase was destabilised at this dopant concentration.

In both thicknesses, the difference in the temperature interval between the Iso-N and N-N_F phase transition temperatures remained relatively constant between concentrations, maintaining an average interval of 58.5 °C. Thus, increasing the doping concentrations causes the phase transition temperatures to be lowered by a relatively equal factor, that is to say, the relationship is linear. Furthermore, it is observed that the thinner CRC has slightly lower transition temperatures, of about 5 °C, compared to that of the thicker cell.

Finally, phase transition temperatures were only measured for cooling down of the sample and not for heating up. This distinction needs to be made as it was observed throughout the experiment that the N-N_F phase transition occurred at higher temperatures when heating up as opposed to cooling down of the LC. Similar observations were made in the report by Feng et al. [6] however, this project did not further investigate this phenomenon and focused on the cooling down sequences.

4.2 Pitch Measurements

Figure 4.2 shows a complete cycle of cooling for the 1.5 μm CRC filled with 0.9 wt% S811 in RM734, the top cell is UR. As expected, the disclination lines behave similarly to that of prior studies [8][9]. In the N phase the disclination line rotates at a deviation angle away from the rubbing axis as the temperature decreases. In this case, it moves counterclockwise. Once the N-N_F transition temperature is met, the two N disclination lines come together and form one N_F disclination line roughly at the normal to the N phase's disclination lines. Following this comes the first significant result; when the temperature continues to decrease after the N-N_F transition, then as theorised, the N_F phase disclination line continues to make a counterclockwise turn as the temperature continues to decrease. Thus the pitch can be calculated from the deviation angle in the N_F phase.

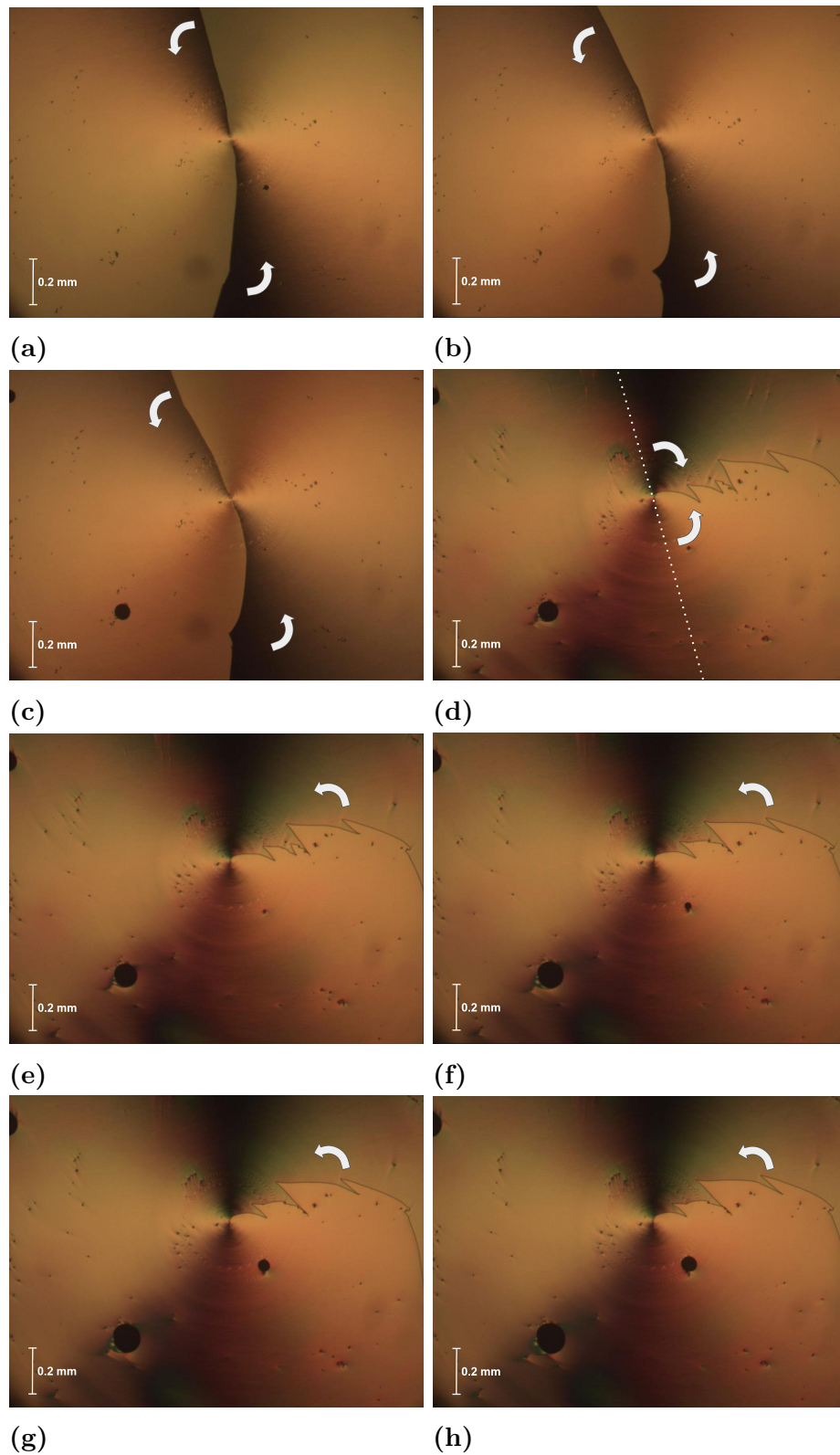


Figure 4.2: Images showing disclination lines of 0.9 wt% doped 1.5 μm CRC at different temperatures **a)** 170 $^{\circ}\text{C}$, **b)** 150 $^{\circ}\text{C}$, **c)** 130 $^{\circ}\text{C}$, **d)** 120 $^{\circ}\text{C}$, **e)** 115 $^{\circ}\text{C}$, **f)** 105 $^{\circ}\text{C}$, **g)** 95 $^{\circ}\text{C}$ and **h)** 85 $^{\circ}\text{C}$ for the cooling down of the cell. The white arrows indicate the disclination lines movement.

In many of the cells, the disclination line begins to bend the further away from the core of the cell the line is. A reason for this could be that the CR rubbing only took place on a small portion in the middle of the cell. This would mean that the rubbing effect is weaker at the outer edges of the rubbing and thus the effect is less pronounced.

Furthermore, the N_F phase disclination line is noted to be jagged and "z" like in its appearance, this is similar to the disclination lines found in antiparallel cells and are representative of antiparallel domains [20].

4.2.1 Calculations and Observations

Consider now the results for the N case depicted in Figure 4.3a), which shows a $1.5 \mu\text{m}$ thick CRC filled with 0.9 wt% S811 in RM734 at 170°C as obtained from the experiment. In accordance with the method, the angle is measured from the deviation to the rubbing line and the pitch is calculated from Equation 2.4. In this case, the angle of deviation is 103° , which means that the molecular directors at either side of the disclination line make either a 193° or 13° rotation, see Figure 4.3b). For this deviation angle, the pitch is calculated to be roughly $5.2 \mu\text{m}$ and is left-handed.

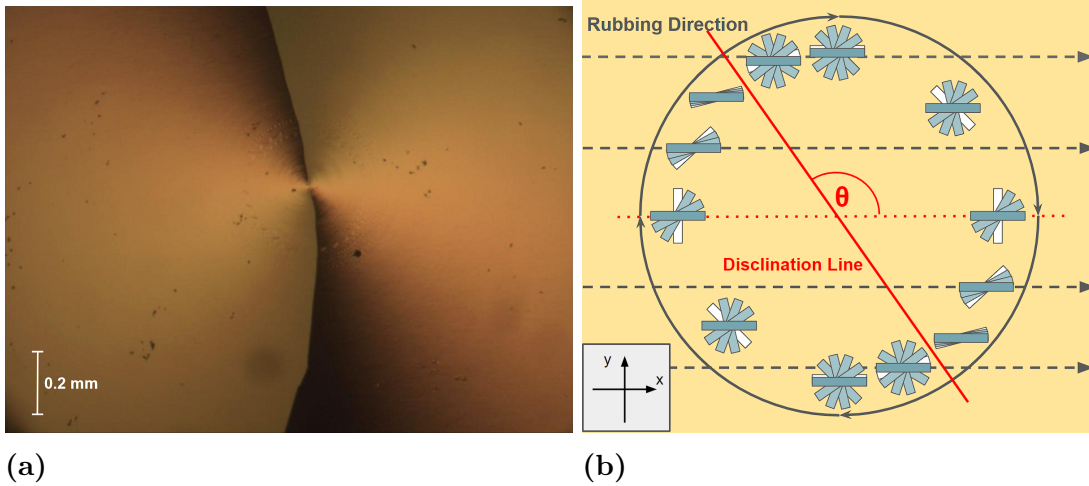


Figure 4.3: Figures showing **a)** $1.5 \mu\text{m}$ thick CRC filled with 0.9 wt% S811 in RM734 at 170°C showing disclination line, image captured by the POM camera. **b)** Schematic representation of the POM image showing the director twist in the molecules.

Similarly, this process is repeated for the N_F phase. Figure 4.4 shows the same cell but at 120°C . Now, the angle of deviation is 105° resulting in a pitch of $5.1 \mu\text{m}$ that is left-handed. The molecular directors on either side of the disclination line would make either a 285° or 75° rotation.

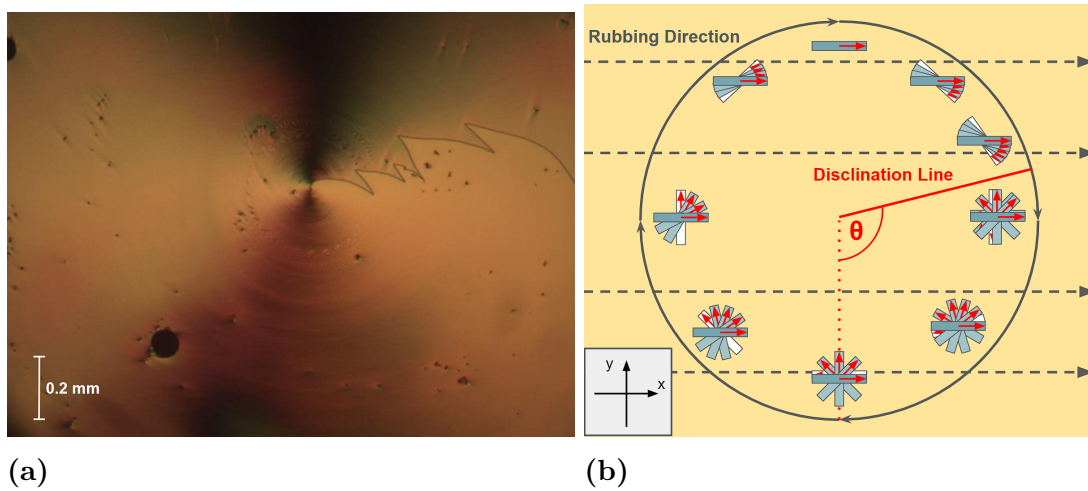


Figure 4.4: Figures showing **a)** 1.5 μm thick CRC filled with 0.9 wt% S811 in RM734 at 120 $^{\circ}\text{C}$ showing disclination line, image captured by the POM camera. **b)** Schematic representation of the POM image showing the director twist in the molecules.

These measurements and calculations are performed for all the different temperature intervals tested and the results are presented below in Table 4.1. For further details regarding the angle measurements see Figure A.1 in the Appendix.

T ($^{\circ}\text{C}$)	Observed Angle (degrees)	p (μm)
170	103	5.2
150	114	4.7
130	116	4.7
120	105	5.1
115	107	5.0
105	110	4.9
95	111	4.9
85	113	4.8

Table 4.1: Table showing the obtained deviation angles of the disclination lines and pitch for the 1.5 μm CRC at different temperatures of 0.9 wt% doping.

Here it is seen that the disclination angle decreases with increasing temperature, leading to an increase in the pitch. Just like the transition phase temperatures, the pitch values obtained here are similar to that obtained by Feng et al. at about 5 μm . Although this project is the first to measure the N_F pitch by use of the CRC method.

The resulting pitches of the 1.5 μm CRC are used to predict the deviation angles of the 4 μm CRC. These are then compared to the actual observed values, the results for which are listed in Table 4.2. For further details see Figure A.2.

4. Results

T (°C)	Predicted Angle (degrees)	Observed Angle (degrees)	p (μm)
170	275	43	6.5
150	304	53	6.3
130	309	46	6.4
120	280	8	7.7
115	285	16	7.3
105	293	21	7.2
95	296	26	7.0
85	301	29	6.9

Table 4.2: Table showing the predicted and observed deviation angles as well as resulting pitch for the $4\ \mu\text{m}$ CRC at different temperatures of 0.9 wt% doping.

The observed angles are vastly different from the predicted ones, however, this could potentially be explained if the assumption is made that the molecules are undergoing additional half rotations in the $4\ \mu\text{m}$ cell. Recall Section 2.5.3 where it was stated that "the angles θ and $\theta + n\pi$, where n is an integer, although corresponding to two different pitches will display the same apparent disclination line". Bearing this in mind, if a correction is made by adding a rotation of 180° or 360° to the observed results the predicted and observed angles will match each other significantly better.

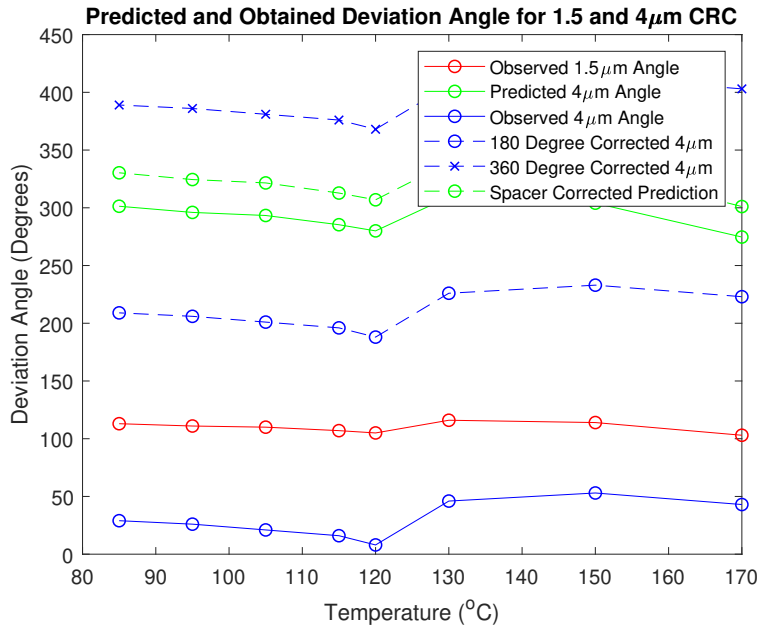


Figure 4.5: Plot of the predicted, observed and corrected disclination line angles in the 1.5 and $4\ \mu\text{m}$ CRC.

Figure 4.5 shows the values obtained in Tables 4.1 and 4.2. As can be seen, when corrected with 180° the resulting deviation angle matches the predicted $4\ \mu\text{m}$ angle much better than the observed one. It is also a better fit than the 360° correction by a small margin. However, it needs to be addressed that the cell gap d may actually be smaller than what is given by the glass spacers. This is because the vacuum

sealing may forcefully cause the UR or CR cells to slightly bend inwards. Thus, if the cell gap is chosen to be 1.3 and 3.8 μm instead of 1.5 and 4 μm respectively. Then the results indicate that the 360° correction is a better fit to the predicted angles. These trends are mimicked in the pitch calculations.

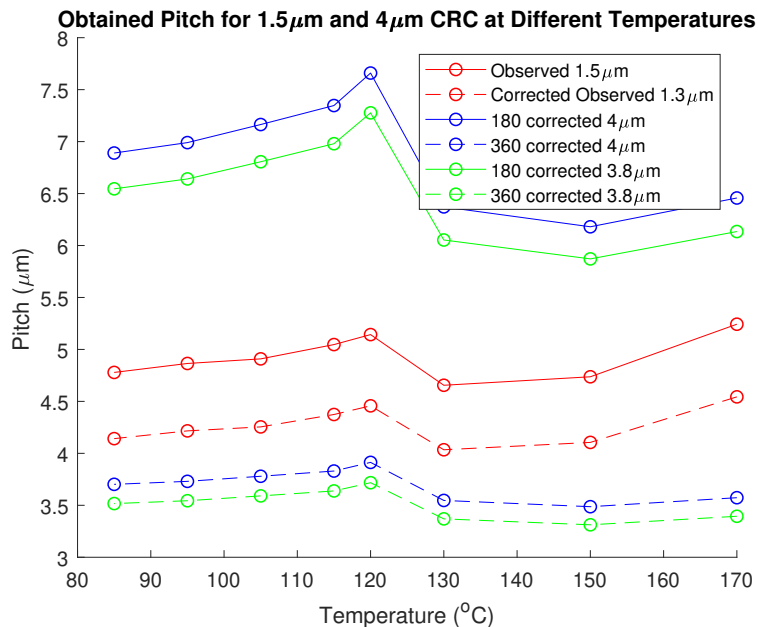


Figure 4.6: Plots of the calculated pitch values from the observed and corrected disclination angles of the 1.5 and 4 μm CRC at different temperatures.

In Figure 4.6 the plots for the calculated pitches from the observed and corrected disclination lines are presented. These results indicate an increase in pitch as the temperature increases. There is, however, a sudden drop in pitch as the material enters the N_F before the pitch increases once again. Here, the 360° correction is the best fit from the start as it is closest in value to the 1.5 μm pitch. In this case, correcting for the spacers only results in an even better fit.

However despite this, for both the cell thicknesses, the predicted pitch and disclination angles are still relatively far off from the observed ones. One could speculate that the explanation for this may come from a study by Khachatryan [7] who predicted that the N_F phase could spontaneously form a helix. If the dipole interactions in the N_F phase affect the pitch, then it could be expected that there is a larger difference between the pitches of the N and N_F phases.

A final point worth noting is that for cells where the deviation of the disclination line is larger than $\pi/2$, there is no longer any right-handed twist in the cell, that is to say, the helix is left-handed. This was a recurring phenomenon in the experiments conducted, the left-handed twist became dominant over the right-handed as the director rotation increased. The effect of this twist can be seen with the POM, as the darker regions diminish due to the increased twist of the director. This effect is more pronounced for the concentrations tested above 0.9 wt%. In these cells, the director twist is too large for accurate measurements on the pitch to be made since

the director rotates more than 180° . As can be seen in Figure 4.7 the large twist results in no dark regions of complete extinction in the CRC when viewed in the POM as the molecules never make the small twists required for complete darkness.

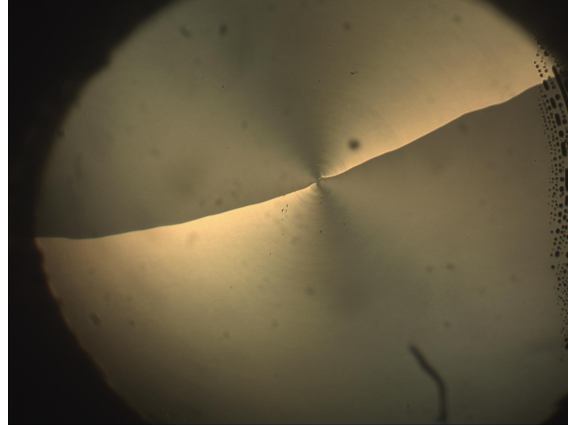


Figure 4.7: *POM image of a $1.5 \mu\text{m}$ CRC filled with 3.0 wt% S811 in RM734 under crossed polarisers at 170°C .*

4.3 Polymer Stabilisation

The results of the polymer stabilisation are surprising as contrary to expectations, the UV-treated LC does not conclusively exhibit stabilisation. Yet there are indications that there is some disturbance to the LC sample, although the reason for this remained undetermined.

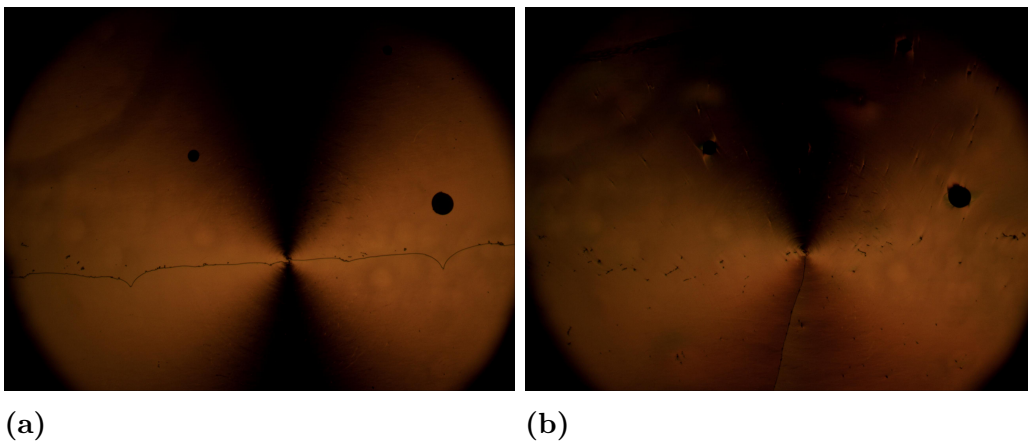


Figure 4.8: *POM images of $1.5 \mu\text{m}$ CRC filled with pure RM734, Irgacure 651 and RM82 at **a)** 150°C and **b)** 110°C before UV exposure.*

Obtained in Figure 4.8 are the POM images of a $1.5 \mu\text{m}$ CRC filled with a mixture of pure RM734, Irgacure 651 and RM82 at 150°C and 110°C before UV exposure. As can be seen, the cell displays the characteristic N and N_F disclination lines at the corresponding temperatures. By exposing this cell to UV light at 150°C . The

cell should in theory be stabilised at the N phase and remain displaying these disclination lines when cooled down to the N_F transition temperature.

But this is not the case, as can be seen in Figure 4.9. After UV exposure, at 150°C the cell still exhibits the N disclination line as expected. However, when cooling down to the N_F the sample does not remain in the N phase as it should if it were successfully stabilised. Instead, it begins to form an incomplete N_F disclination line. As is evident in Figure 4.9b) the disclination line begins to take a N_F shape before abruptly making an orthogonal turn along the rubbing direction. The line also displays the antiparallel jagged "z" line as previously seen in the doped CRCs but not in the pure RM734.

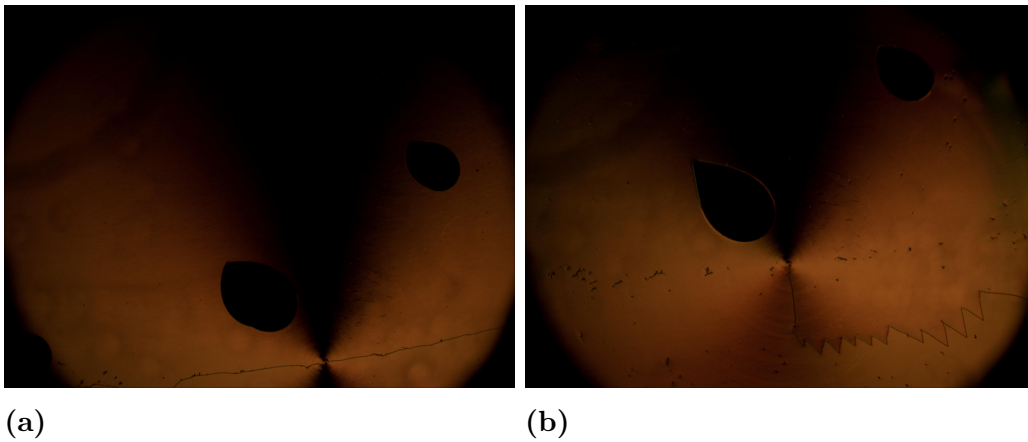


Figure 4.9: *POM images of $1.5\ \mu\text{m}$ CRC filled with pure RM734, Irgacure 651 and RM82 at a) 150°C and b) 110°C after UV exposure.*

The reasons for why polymer stabilisation does not occur here are unknown, however, there are a few suggestions. The first of which is that there is simply an insufficient amount of UV photoinitiator used and that a higher concentration is required in order to achieve polymer stabilisation. It is also possible that the UV exposure simply missed the sample completely, as it was hard to accurately select the area to be exposed. Furthermore, it is also possible that the sample was not exposed at the right temperature, as the UV exposure inadvertently heats up the sample. Finally, polymer stabilisation may not have occurred because the polymer may have moved to the surface or the monomer may have been separated from the mixture. There was unfortunately not enough time to further explore this behaviour of the polymer stabilisation in this project.

5

Conclusion

In conclusion, this project has explored and for the first time, successfully performed pitch measurements on the N_F phase by use of the CRC method. The method is still unrefined and there are issues with accuracy, but further development is likely to improve this aspect. The effects that chiral dopant S811 has on the N_F material RM734 have also been investigated. The results of the experiment have shown that similarly to the N phase, the N_F disclination line in a CRC twists around the rubbing axis and that pitch can be calculated from the resulting deviation angle by means of Equation 2.4. The resulting pitch is in accordance with previous pitch measurements performed using other methods. However, the CRC method opens up the possibility of measuring long pitch at much lower doping concentrations. The results have further provided evidence supporting previous studies of the negative trend in doping concentration and phase transition temperatures of chiral dopant S811 and RM734. Furthermore, it was observed that the pitch in the CRCs increases with temperature and with cell thickness. Finally, it was seen that as the material reaches the N- N_F phase transition the pitch experiences a sudden drop in length before increasing again.

Further research is necessary to confirm if the results of this experiment are case specific to the RM734 material or if they can be applied to all other N_F materials. Future research should also focus on the effects of varying the cell gap and using even smaller and more accurate doping concentrations. Testing of higher photoinitiator concentrations for the polymer stabilisation attempt should also be made.

Nevertheless, the results from this report reveal the intriguing properties of N_F LCs and provide a new method for pitch measuring, of which further investigation into N_F LC materials can be made.

Bibliography

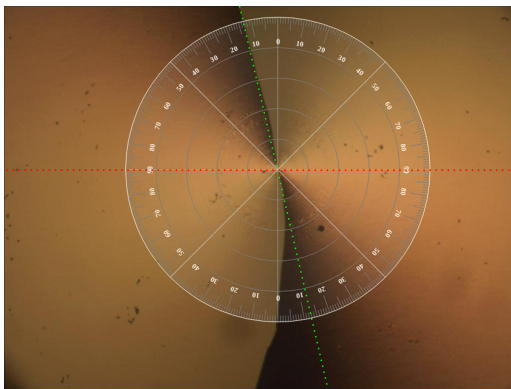
- [1] Xi Chen et al. “First-principles experimental demonstration of ferroelectricity in a thermotropic nematic liquid crystal: Polar domains and striking electro-optics”. In: *Proceedings of the National Academy of Sciences* 117.25 (June 2020), pp. 14021–14031. DOI: [10.1073/pnas.2002290117](https://doi.org/10.1073/pnas.2002290117). URL: <https://doi.org/10.1073/pnas.2002290117>.
- [2] Hiroya Nishikawa et al. “A Fluid Liquid-Crystal Material with Highly Polar Order”. In: *Advanced Materials* 29.43 (Nov. 2017), p. 1702354. ISSN: 0935-9648. DOI: <https://doi.org/10.1002/adma.201702354>. URL: <https://doi.org/10.1002/adma.201702354>.
- [3] Richard J Mandle, Stephen J Cowling, and John W Goodby. “Rational Design of Rod-Like Liquid Crystals Exhibiting Two Nematic Phases”. In: *Chemistry – A European Journal* 23.58 (Oct. 2017), pp. 14554–14562. ISSN: 0947-6539. DOI: <https://doi.org/10.1002/chem.201702742>. URL: <https://doi.org/10.1002/chem.201702742>.
- [4] Richard J Mandle, S J Cowling, and J W Goodby. “A nematic to nematic transformation exhibited by a rod-like liquid crystal”. In: *Physical Chemistry Chemical Physics* 19.18 (2017), pp. 11429–11435. ISSN: 1463-9076. DOI: [10.1039/C7CP00456G](https://doi.org/10.1039/C7CP00456G). URL: <http://dx.doi.org/10.1039/C7CP00456G>.
- [5] Nerea Sebastián et al. “Ferroelectric-Ferroelastic Phase Transition in a Nematic Liquid Crystal”. In: *Phys. Rev. Lett.* 124 (3 Jan. 2020), p. 037801. DOI: [10.1103/PhysRevLett.124.037801](https://doi.org/10.1103/PhysRevLett.124.037801). URL: <https://link.aps.org/doi/10.1103/PhysRevLett.124.037801>.
- [6] Chenrun Feng et al. “Electrically Tunable Reflection Color of Chiral Ferroelectric Nematic Liquid Crystals”. In: *Advanced Optical Materials* 9.22 (2021), p. 2101230. DOI: <https://doi.org/10.1002/adom.202101230>. URL: <https://onlinelibrary.wiley.com/doi/abs/10.1002/adom.202101230>.
- [7] A.G. Khachatryan. “Development of helical cholesteric structure in a nematic liquid crystal due to the dipole-dipole interaction”. In: *Journal of Physics and Chemistry of Solids* 36.10 (1975), pp. 1055–1061. ISSN: 0022-3697. DOI: [https://doi.org/10.1016/0022-3697\(75\)90044-X](https://doi.org/10.1016/0022-3697(75)90044-X). URL: <https://www.sciencedirect.com/science/article/pii/002236977590044X>.
- [8] Per Rudquist. “Revealing the polar nature of a ferroelectric nematic by means of circular alignment”. In: *Scientific Reports* 11.1 (2021), p. 24411. ISSN: 2045-2322. DOI: [10.1038/s41598-021-04028-7](https://doi.org/10.1038/s41598-021-04028-7). URL: <https://doi.org/10.1038/s41598-021-04028-7>.
- [9] Seong-Woo Suh et al. “Precise determination of the cholesteric pitch of a chiral liquid crystal in a circularly aligned configuration”. In: *Applied Physics Letters*

- 70.19 (May 1997), pp. 2547–2549. ISSN: 0003-6951. DOI: 10.1063/1.118916. URL: <http://aip.scitation.org/doi/10.1063/1.118916>.
- [10] I. Dierking. *Polymer-modified Liquid Crystals*. Soft Matter Series. Royal Society of Chemistry, 2019. ISBN: 9781782629825. URL: <https://books.google.se/books?id=U1WCDwAAQBAJ>.
- [11] P J Collings and J W Goodby. *Introduction to Liquid Crystals: Chemistry and Physics, Second Edition*. CRC Press, 2019. ISBN: 9781351579827. URL: <https://books.google.se/books?id=EJu4DwAAQBAJ>.
- [12] Nerea Sebastián, Martin Čopič, and Alenka Mertelj. “Ferroelectric nematic liquid-crystalline phases”. In: *Phys. Rev. E* 106 (2 Aug. 2022), p. 021001. DOI: 10.1103/PhysRevE.106.021001. URL: <https://link.aps.org/doi/10.1103/PhysRevE.106.021001>.
- [13] Alenka Mertelj et al. “Splay nematic phase”. In: *Physical Review X* 8.4 (2018), p. 041025.
- [14] Richard J Mandle and Alenka Mertelj. “Orientational order in the splay nematic ground state”. In: *Physical Chemistry Chemical Physics* 21.34 (2019), pp. 18769–18772.
- [15] Perri LM Connor and Richard J Mandle. “Chemically induced splay nematic phase with micron scale periodicity”. In: *Soft Matter* 16.2 (2020), pp. 324–329.
- [16] M. Kléman. “Defects in Liquid Crystals”. In: ed. by Glenn H. Brown. Vol. 1. *Advances in Liquid Crystals*. Elsevier, 1975, pp. 267–311. DOI: <https://doi.org/10.1016/B978-0-12-025001-1.50011-1>. URL: <https://www.sciencedirect.com/science/article/pii/B9780120250011500111>.
- [17] E. Hecht. *Optics*. Always learning. Pearson, 2016. ISBN: 9781292096933. URL: <https://books.google.se/books?id=Bv1RrgEACAAJ>.
- [18] K. Takato et al. *Alignment Technology and Applications of Liquid Crystal Devices*. Liquid Crystals Book Series. Taylor & Francis Group, 2019. ISBN: 9780367392475. URL: <https://books.google.se/books?id=g2igyAEACAAJ>.
- [19] Xi Chen et al. “Polar in-plane surface orientation of a ferroelectric nematic liquid crystal: Polar monodomains and twisted state electro-optics”. In: *Proceedings of the National Academy of Sciences* 118.22 (2021), e2104092118. DOI: 10.1073/pnas.2104092118. eprint: <https://www.pnas.org/doi/pdf/10.1073/pnas.2104092118>. URL: <https://www.pnas.org/doi/abs/10.1073/pnas.2104092118>.
- [20] Federico Caimi et al. “Surface alignment of ferroelectric nematic liquid crystals”. In: *Soft Matter* 17.35 (2021), pp. 8130–8139.
- [21] Jeong-Seon Yu et al. “Alignment properties of a ferroelectric nematic liquid crystal on the rubbed substrates”. In: *Soft Matter* 19 (13 2023), pp. 2446–2453. DOI: 10.1039/D3SM00123G. URL: <http://dx.doi.org/10.1039/D3SM00123G>.
- [22] Damian Pocięcha et al. “Intrinsically chiral ferronematic liquid crystals: An inversion of the helical twist sense at the chiral nematic – Chiral ferronematic phase transition”. In: *Journal of Molecular Liquids* 361 (2022), p. 119532. ISSN: 0167-7322. DOI: <https://doi.org/10.1016/j.molliq.2022.119532>. URL: <https://www.sciencedirect.com/science/article/pii/S0167732222010704>.

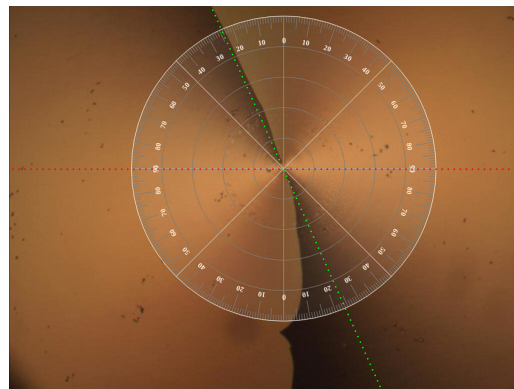
A

Measurements of Deviation Angles

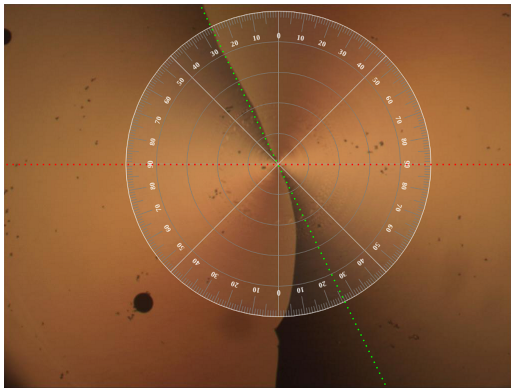
This appendix show POM images of the CRCs and how the deviation angles for them were obtained.



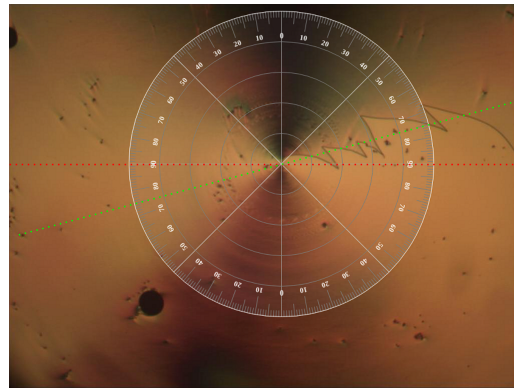
(a)



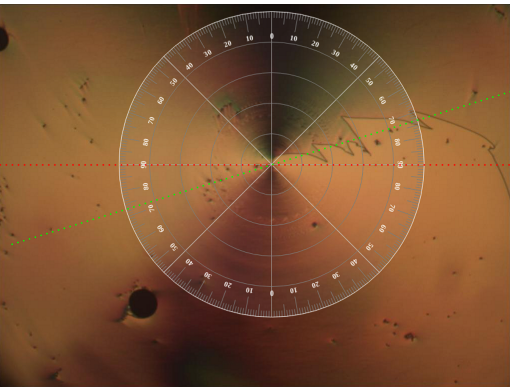
(b)



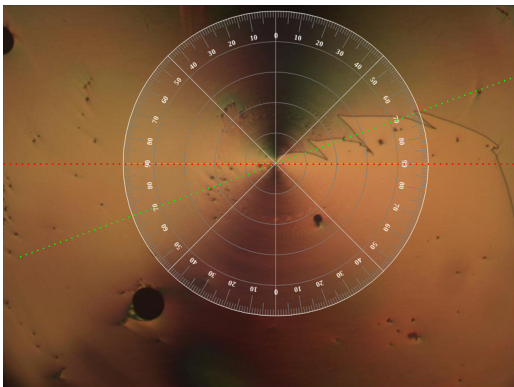
(c)



(d)

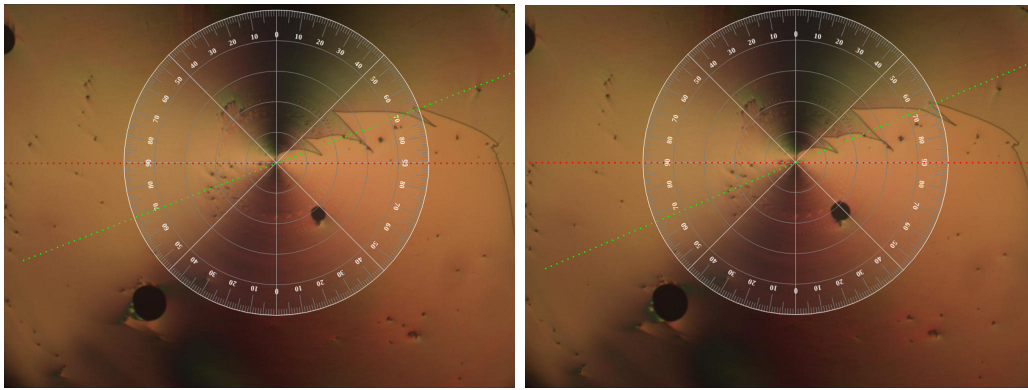


(e)



(f)

A. Measurements of Deviation Angles

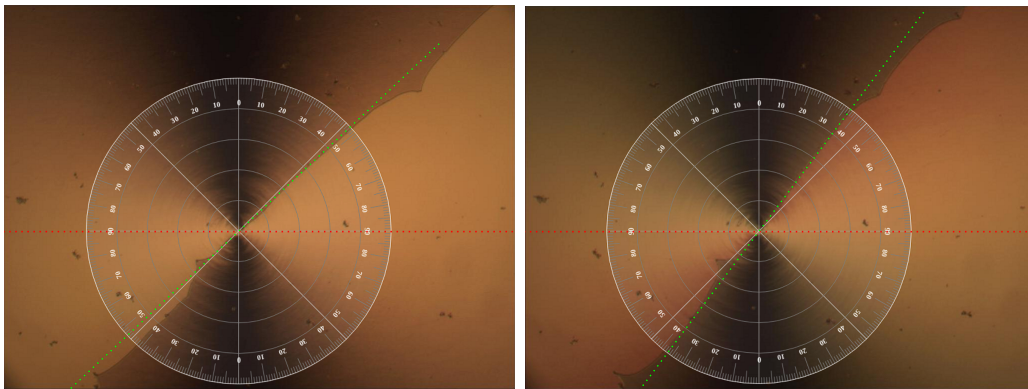


(g)

(h)

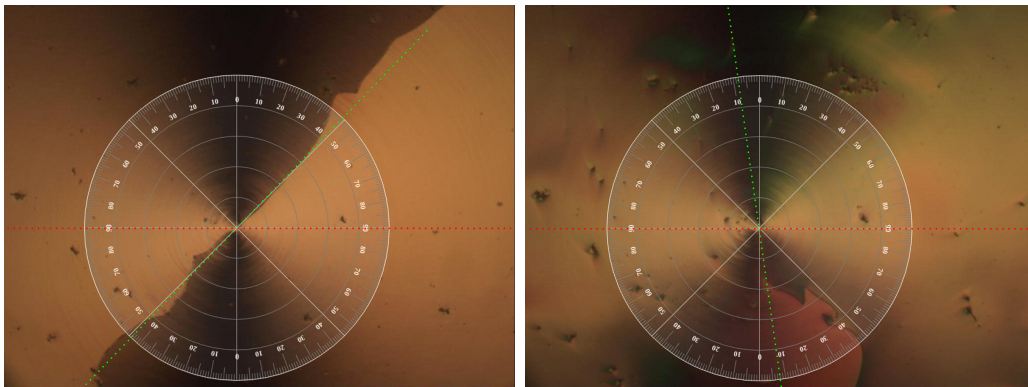
Figure A.1: POM images of the $1.5\mu\text{m}$ CRC filled with $0.9\text{wt}\%$ doping concentration at different temperatures **a)** 170°C , **b)** 150°C , **c)** 130°C , **d)** 120°C , **e)** 115°C , **f)** 105°C , **g)** 95°C and **h)** 85°C . The dotted red line is the rubbing axis and the green line is an approximation for the disclination line. Using the circular protractor the angle is measured.

Figure A.1 shows the measurements for the $1.5\mu\text{m}$ CRC of which the results were presented in Table 4.1. Figure A.2 shows the measurements for the $4\mu\text{m}$ CRC of which the results were presented in Table 4.2.



(a)

(b)



(c)

(d)

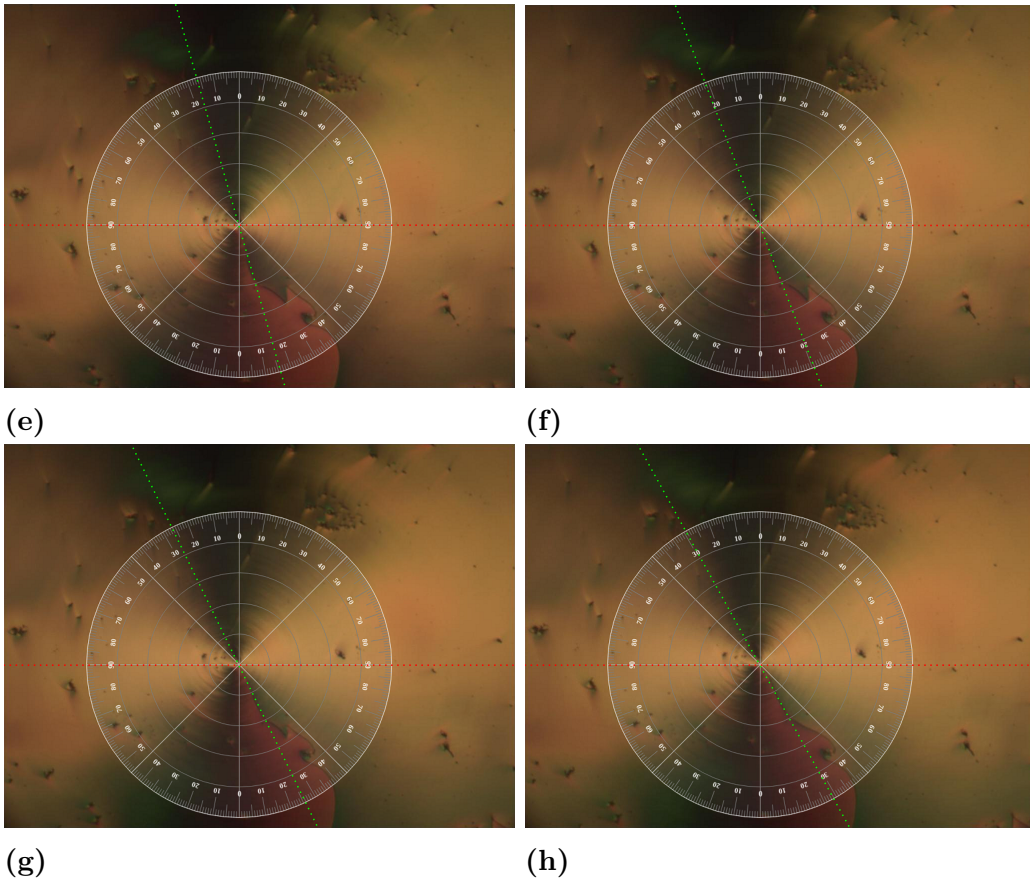


Figure A.2: POM images of the $4\mu\text{m}$ CRC filled with $0.9\text{wt}\%$ doping concentration at different temperatures **a)** 170°C , **b)** 150°C , **c)** 130°C , **d)** 120°C , **e)** 115°C , **f)** 105°C , **g)** 95°C and **h)** 85°C . The dotted red line is the rubbing axis and the green line is an approximation for the disclination line. Using the circular protractor the angle is measured.

DEPARTMENT OF MICROTECHNOLOGY AND NANOSCIENCE
CHALMERS UNIVERSITY OF TECHNOLOGY
Gothenburg, Sweden
www.chalmers.se



CHALMERS
UNIVERSITY OF TECHNOLOGY